

**Quantifying and Correlating the Positive Airway Pressure and Upper Airway Gas Clearance During High Flow Nasal Cannula Therapy in Adults**

By

Charles Paul Moore

A thesis submitted in partial fulfillment of the requirements for the degree of

Master of Science

Department of Mechanical Engineering

University of Alberta

©Charles Paul Moore, 2019

## **Abstract**

High flow nasal cannula (HFNC) therapy is a form of respiratory support, where high flowrates of heated and humidified gas are supplied to a patient via nasal cannula. This thesis consists of two experimental studies designed to characterize the positive pressure and upper airway washout effects of HFNC therapy. We characterized these effects by supplying HFNC to five plastic adult airway replicas, extending from the nares to trachea. The first set of experiments measured airway washout in a non breathing model, comparing 3 cannula and HFNC flowrates of 30-90 L/min. Pressure was measured by connecting the airways to a lung simulator and delivering HFNC therapy, with flowrates of 0-60 L/min. Post-hoc analysis revealed clearance times decreasing with increasing flowrate and decreasing cannula size. A predictive correlation for positive end expiratory pressure (PEEP) was developed using a minor losses model of confined flow. The second set of experiments involved simulating breathing with CO<sub>2</sub> production in the lungs during HFNC administration. Flowrates ranged from 0-60 L/min of either air, pure oxygen or heliox gas. Washout of CO<sub>2</sub> in the airways was heavily dependent upon HFNC flowrate, and weakly dependent upon gas and airway geometry. Washout effect was found to be independent of breathing minute volume. A second correlation for PEEP was constructed based on minor losses, and accounting for differing gas density.

## **Dedication**

I would like to dedicate the present work to my grandfather. No other academic has brought me so much joy. No other academic will be so missed.

## **Acknowledgements**

First and foremost, I would like to thank my supervisor, Dr Andrew Martin. When I was an undergraduate student, I had the opportunity to be one of the first students to work in his lab as a summer researcher. By the end of those four months, I was absolutely certain that I wanted to pursue a graduate degree. I consider myself exceptionally fortunate to have found a supervisor I liked working with so much, so quickly. When I was in a difficult spot, even when it affected my work, he was always supportive and understanding. Whenever a new opportunity arose, he encouraged me to pursue it. Thank you for guiding me, as an undergraduate and graduate student. Your insight and guidance has been invaluable and I can think of no better role model as a researcher and teacher than you.

I would also like to express my gratitude to Dr Warren Finlay. Your contribution to the research contained within this thesis was invaluable. In addition to helping me understand my own research, you helped expand my horizons beyond research into high flow therapy. The work I did under your supervision is a highlight of my time as a graduate student.

I would like to thank my other co-authors of the pieces contained within this thesis, Dr Ira Katz, Dr Marine Pichelin and Dr Georges Caillibotte. Without their contribution, the works contained within would not be what they are. I would also like to extend my gratitude for their part in introducing me to the wider world of respiratory support research.

In addition to Dr Martin and Dr Finlay, I would like to thank the rest of my committee members, Dr Hossein Rouhani and Dr Peichun Amy Tsai. Your time and feedback is greatly appreciated.

I would like to thank all the members of the aerosol research lab and respiratory mechanics lab for their support during my time here. To Scott Tavernini, Milad Kiaee, Alvin Ly and Conor Ruzycki, thank you for your help understanding aerosol deposition within upper airway replicas. To John Chen, I would like to extend a great thanks for your help in using the lung simulation equipment, even when I had to have the same procedures explained every few months. Tyler Paxman, for sitting next to me for two years, and helping me with all of our courses, especially those long nights writing our CFD codes. Finally, I would like to thank Kineshta Pillay, even though I started my research a year before I can't imagine having a greater help. You've been a great support and an incredible friend and I wouldn't have survived that last push to finish writing without you.

My family have been an incredible support at every stage of my education. Whenever I needed help, you were there to help me. You taught me to value learning, and the values and life philosophy I have today are because of your guidance. I have missed my parents every day I have lived in Edmonton. Thank you for helping make me who I am today.

Finally, I would like to acknowledge the financial support from the Natural Sciences and Engineering Research Council of Canada (NSERC), Alberta Economic Development and Trade and funding from Air Liquide. Their generous financial support made the work in this thesis possible.

Charles Paul Moore

November 2<sup>nd</sup>, 2018

Edmonton, AB, Canada

# Contents

Chapter 1 Introduction.....	1
Overview.....	1
<i>Respiratory Failure</i> .....	1
<i>Intubation and Other Uses</i> .....	2
<i>Positive Airway Pressure</i> .....	3
<i>Upper Airway Washout</i> .....	5
<i>Human Physiology</i> .....	6
<i>Variable Aspects of HFNC delivery</i> .....	7
<i>Fluid Mechanics</i> .....	8
Purpose of Research.....	13
Thesis Structure.....	14
Chapter 2 Correlation of High Flow Nasal Cannula Outlet Area and Flow with Non-Breathing Gas Clearance and Positive Pressure in Adult Upper Airway Replicas.....	15
Introduction.....	15
Methods.....	18
<i>Nasal Airway Replicas</i> .....	18
<i>Gas Clearance Measurements</i> .....	19
<i>Distending Pressure Measurements</i> .....	24
<i>Statistical Methods</i> .....	25
Results.....	25
<i>Clearance Time</i> .....	25
<i>Distending Pressure</i> .....	27
Discussion .....	28
<i>Cannula Clearance Performance</i> .....	28
<i>Cannula Distending Pressure</i> .....	31
<i>Study Limitations</i> .....	35
Conclusions.....	35
Chapter 3 High Flow Nasal Cannula: Influence of Gas Type and Flow Rate on Airway Pressure and CO <sub>2</sub> Clearance in Adult Nasal Airway Replicas .....	37
Introduction.....	37
Methods.....	39
<i>Experimental Setup</i> .....	39

<i>Influence of breathing pattern</i> .....	44
<i>Analytical Methods</i> .....	44
<b>Results</b> .....	45
<i>Clearance</i> .....	45
<i>Effect of Minute Volume</i> .....	49
<i>Pressure</i> .....	50
<b>Discussion</b> .....	52
<i>Factors Influencing Gas Clearance</i> .....	52
<i>Minute Volume Effect on CO<sub>2</sub> Clearance</i> .....	54
<i>Constructing a Predictive Model for Pressure</i> .....	54
<b>Conclusion</b> .....	56
<b>Chapter 4 Conclusions and Recommendations</b> .....	57
<b>Summary</b> .....	57
<b>Future Work</b> .....	58
<b>Works Cited</b> .....	60
<b>Appendix A Raw Data for Chapter 2</b> .....	68
<b>Appendix B Raw Data for Chapter 3</b> .....	75

## List of Figures

<i>Figure 1-1: A diagram of flows into and out of an upper airway between breaths. Blue arrows represent possible sample streamlines, but are not to be taken as to scale. ....</i>	<i>11</i>
<i>Figure 2-1: Side and front view of upper airway replica. Specific replica shown corresponds to "Subject 2".....</i>	<i>18</i>
<i>Figure 2-2: A diagram of the dead space clearance model. Oxygen is supplied from the HFNC gas supply, which replaces the air normally within the airway replica. The gas analyzer sample line is placed at the exit of the model, located at the trachea, or within the model at the larynx. ....</i>	<i>21</i>
<i>Figure 2-3: Cannula used in testing. Shown are large (top), medium (middle) and small (bottom) cannula.....</i>	<i>22</i>
<i>Figure 2-4: Average clearance times of all subjects, from 25% to 75% oxygen, sampled at the trachea (left) and larynx (right). Error bars represent the propagated standard deviations of the subject means (n=5). ....</i>	<i>26</i>
<i>Figure 2-5: Average pressures of 5 subjects (n=3), measured at cycle maximum (top, left), cycle minimum (top, right), cycle mean (bottom, left) and positive end of expiration pressure (PEEP) (bottom, right). Pressures extracted from pressure waveform over 5 breaths measured by the mechanical lung to approximate tracheal pressure in breathing subjects. Error bars represent the propagated standard deviations of the subject means (n=5). Note: 1 cmH<sub>2</sub>O = 98.07 Pa. ...</i>	<i>27</i>
<i>Figure 2-6: Clearance time as a function of Re measured at the subject cannula. Panels in descending order correspond so subject 2, 5, 6, 8 and 9. Reynolds number determined as described in Equation (2-1). Error bars represent 1 standard deviation for test point (n=5). ....</i>	<i>29</i>
<i>Figure 2-7: A comparison of measured PEEP and PEEP predicted by equation (2-6). Error bars represent 1 standard deviation of PEEP measured at the trachea (n=3) .....</i>	<i>34</i>
<i>Figure 3-1: Diagram of experimental setup, HFNC therapy on an upper airway replica served by a breathing lung simulator. ....</i>	<i>39</i>
<i>Figure 3-2: Sample CO<sub>2</sub> concentration (top) and lung volume (bottom) waveforms for the airway replica of subject 2, without HFNC. Alignment of time axes between the two plots was estimated by visual inspection. ....</i>	<i>42</i>

*Figure 3-3: Average CO<sub>2</sub> per breath, averaged for all replicas, is presented for different cannula and gas type. Error bars represent standard deviation around the average (n = 5). ..... 46*

*Figure 3-4: Average CO<sub>2</sub> concentration over the breath is compared for individual airway replicas for air, heliox, and oxygen. Values compared were obtained using the Vapotherm Adult Cannula, at 60 LPM flow. Geometry numbers correspond with those listed in Table 3-1. Error bars represent one standard deviation (n=3). ..... 47*

*Figure 3-5: A comparison of estimated inhaled volume of CO<sub>2</sub> and average tracheal CO<sub>2</sub>. ..... 48*

*Figure 3-6: Average CO<sub>2</sub>/breath for the replica geometry of subject 2, using the Vapotherm Adult cannula, with modified breathing patterns. Error bars represent standard deviation of the average of 3 repetitions. .... 49*

*Figure 3-7: Average relative normalized CO<sub>2</sub>/breath for replica subject 2 geometry, using Vapotherm Adult cannula, with modified breathing patterns. CO<sub>2</sub> normalized to data at 0 L/min HFNC flow. Error bars omitted for clarity, see Figure 3-6 for relative uncertainties in measurement. .... 50*

*Figure 3-8: Average PEEP for all replica geometries, controlled for cannula and gas selection, compared with HFNC flowrate. Trendlines presented for individual case quadratic best fit. Error bars represent standard deviation around the average (n = 5). ..... 51*

*Figure 3-9: Comparison of PEEP with respect to flowrate for each airway geometry. Cases compared are breathing air, with Vapotherm® adult cannula selected. Trendlines presented for individual case quadratic best fit. Error bars represent 1 standard deviation, N=3. .... 52*

**List of Tables**

*Table 2-1: Rapid prototyped upper airway replica subject parameters. Data from Golshahi et al. (70) ..... 19*

*Table 2-2: Cannula outlet area, corresponding to the cannula inner diameter, cannula prong outer area, corresponding to the cannula outer diameter, and Reynolds number at tested flow rates exiting the cannula outlet. .... 23*

*Table 3-1: Rapid prototyped upper airway replica dimensions. Data from Golshahi et al. (70) and Moore et al. (79). .... 40*

*Table 3-2 Cannula Dimensions used in HFNC therapy ..... 41*

## **Chapter 1 Introduction**

### **Overview**

High Flow Nasal Cannula (HFNC) therapy, often referred to as high flow therapy, is a relatively recent development form of non-invasive ventilatory support. HFNC operates by supplying high flowrates (>15 L/min in adults) of gas to the nares via nasal cannula to assist breathing (1). HFNC has been used to treat a range of respiratory issues, from alleviating acute respiratory distress, to aiding recovery post-extubation. The gas is heated to body temperature and humidified to saturation, which minimizes patient discomfort from dryness, and decreases the amount of work done to condition the inhaled gas (1-4). Dysart *et al.* describes two of the primary benefits of the therapy are the exhaled gas washout, and positive pressure (1). Other proposed benefits include reducing nasopharyngeal resistance, alveolar recruitment and improving mucociliary clearance, and improved pulmonary compliance (1-4).

### ***Respiratory Failure***

Although hypercapnic respiratory failure is typically treated by non-invasive ventilation (NIV), HFNC is a viable alternative to NIV (2, 3). HFNC has the advantage of not requiring a facemask, and being an open system compared to other forms of respiratory support. It also offers improved outcomes over conventional oxygen delivery. In patients with hypoxemic respiratory failure due to chronic obstructive pulmonary disorder (COPD) PaCO<sub>2</sub> and minute volume was found to decrease when undergoing HFNC (5, 6).

Particularly in the case of hypoxemia and acute respiratory distress syndrome (ARDS), maintaining oxygenation is dependent on maintaining a high enough FiO<sub>2</sub> and Positive End Expiratory Pressure (PEEP) (3). In patients experiencing moderate hypoxemic respiratory failure,

HFNC has shown significant improvement in oxygenation, with a delay of need to intubate, attributed to the positive pressure effect and washout effects (7). In severe cases of respiratory failure HFNC has shown some promise, reducing rate of intubation compared to conventional oxygen, however further evidence is required to establish a clear guideline on use of HFNC in ARDS compared to conventional delivery such as NIV which may offer better oxygenation (8, 9). Meta analyses of HFNC compared to NIV in patients experiencing ARDS found consistently that there was little difference in mortality; however patients did experience better comfort undergoing HFNC (10-12). HFNC offers advantages in patient comfort compared to other therapies, as it lacks the mask of NIV and constant positive airway pressure (CPAP) therapy. Meanwhile, HFNC also has advantages in offering a positive pressure, which conventional oxygen cannula does not offer. In a randomized trial of 310 patients with hypoxemic respiratory failure, Frat *et al.* found that HFNC outperformed both conventional oxygen and NIV with respect to 90 day mortality (13). Accounting for this, HFNC is a promising alternative to other respiratory support therapies treating ARDS, but precise guides on when to select HFNC have yet to be developed.

### ***Intubation and Other Uses***

Post-extubation recovery typically requires respiratory support immediately after in order to prevent reintubation and further respiratory failure. HFNC is associated with a lower respiratory and heart rate, and increased oxygenation during post-extubation (14). A meta-analysis by Zhao *et al.* found that compared to conventional oxygen therapy, HFNC was associated with PaCO<sub>2</sub>, and a reduction in need to reintubate (15). Compared to NIV, which requires a mask, HFNC was found to be non-inferior during initial post-extubation period, with the exception of patient

comfort (15). Due to the open interface of the nasal cannula, it is possible to use HFNC during tracheal intubation without interfering with the laryngoscopy. HFNC has shown promise in preparing pre-intubation patients, showing 100% SpO<sub>2</sub> and reduced severe hypoxemia (16, 17).

As a relatively new therapy, HFNC has several possible uses that are only now being explored. Although CPAP is typically used to treat obstructive sleep apnea, as the pressure prevents upper airway collapse, many patients find CPAP to be too uncomfortable to use regularly. There is some evidence to suggest that HFNC may be an effective treatment for sleep apnea, as the therapy creates a positive pressure in the upper airways, although typically pressures lower than those induced in CPAP (18, 19). Similarly, there is some evidence to suggest that HFNC may be an effective component of regular COPD, owing in part to the increase in PEEP and improved mucocilliary clearance (20).

### ***Positive Airway Pressure***

One benefit proposed consistently of HFNC is the positive airway pressure that is generated. Positive airway pressure is a target of many respiratory support systems, notably CPAP, which maintains a consistent airway pressure, typically ranging from 4-20 cmH<sub>2</sub>O in adults (21). *In vivo* estimates by Parke *et al.* of pressure increase induced from HFNC ranges from 1.5-3.1 cmH<sub>2</sub>O at flowrates of 30-50 L/min (22). Although this pressure is smaller than other therapies, it has been suggested that this positive pressure is sufficient to improve alveolar recruitment, and thereby improve oxygenation and contribute to a reduced breathing frequency (1-4).

Although HFNC is an open interface, unlike CPAP and NIV, the pressures are still significant. It has been suggested that this is due to the partial occlusion of the nares relative to the additional flow from the cannula (1, 23). Frizzola *et al.* compared patients breathing with one

and two prongs inserted into the nares, and found that pressures reduced by approximately 0.5 cmH<sub>2</sub>O (24). Furthermore, both *in vivo* and *in vitro* experiments where patients or models undergoing HFNC breathed with open mouths, showed pressures dropping precipitously, and often to negligible levels, when compared to unassisted breathing (23, 25-30). The occlusion provided during HFNC disappears as the mouth is opened, with a much larger opening in the flow system being provided.

The literature provided on pressure profiles relative to flowrates is varied. Earlier experiments have suggested a linear relationship between increased pressure and HFNC flowrate (26, 31), but these results have been contested. More recent *in vitro* experiments by Nielsen *et al.* and Luo *et al.* also generally suggest a quadratic pressure correlation (29, 30, 32). Modeling a physiologically accurate nasal cavity undergoing HFNC, Miller *et al.* notes that the pressure distribution within the upper airways is not entirely consistent, even within distinct regions of the airway (33).

Consider a simplified model of flow for a patient undergoing HFNC therapy. At the moment between breaths, the only inlet for flow is the cannula, and the only outlet the nares. This means the occlusion of the nares reasonably restricts flow, creating a backpressure. This is supported in *in vivo*, *in vitro* and *in silico* experimentation, where cannula which occlude the nares more result in greater pressures (24, 30, 33). Experiments comparing open and closed mouth breathing reflect this, as well as those comparing one and two pronged cannula, with airway pressures decreasing drastically where there is more area for flow to exit.

### ***Upper Airway Washout***

Another primary benefit of HFNC is the washout of the upper airway deadspace (1-4). During breathing, a volume of exhaled air, which is high in O<sub>2</sub> and low in CO<sub>2</sub>, is trapped in the nasopharyngeal cavity. Due to the open interface, HFNC mixes in fresh gas into the exhaled gas from the nasal cavity, thereby pushing out the exhaled gas. Although in healthy adults this volume is small compared to the overall tidal volume, in some patients, such as those with ARDS where breathing is shallow and rapid, this may have a greater impact. Current *in vivo* experiments have shown a reduction in inhaled CO<sub>2</sub> and more efficient breathing during HFNC therapy (5, 7, 24, 34, 35).

*In vitro* and *in silico* experiments are capable of directly measuring the volume of inhaled oxygen and CO<sub>2</sub> in ways which most *in-vivo* experiments cannot. Airway clearance consistently increases with volumetric flow rate provided by the HFNC (30, 36, 37). At higher flowrates, above 30-40 L/min in adults, these experiments show the advantages of increasing flowrates with respect to diminishing clearance (30).

The specific mechanics of this mixing are not fully understood. Some CFD simulations have shed some light on the mechanisms of gas mixing in the upper airways. Simulations by Van Hove *et al.* demonstrated recirculation in the anterior nasal cannula corresponding with reduction in CO<sub>2</sub> (37). Miller *et al.* found similar vortices, following a central inward flow path, resulting in mixing (33). While the positive pressure effect decreases significantly with open mouthed breathing and less occlusive cannula, the clearance effect is enhanced, with more rapid purging of the nasopharyngeal deadspace (24, 33, 36). This would indicate that the increase in area through which exhaled gas can be forced out of the deadspace will correspond

with a decrease in overall CO<sub>2</sub> content, offering a complete circuit for the flow path, out of the mouth.

### ***Human Physiology***

The respiratory system can be generally subdivided into three sections: the upper, central and lower respiratory tract. The upper respiratory system consists of the airways outside of the lung which bring air to the central airways (38, 39). The central airways consist of conducting “pipes” which bring air to the lower respiratory tract (38, 39). The lower respiratory tract consists of the portion of the lung which performs the gas exchange within the alveoli, diffusing oxygen into the bloodstream, and CO<sub>2</sub> from the bloodstream into the air (39). The smallest airways within the lungs, the respiratory bronchioles, are lined with gas exchanging alveoli, terminating in alveolar sacs. Alveoli themselves are collapsible bubble shaped sections of the lung, covered in networks of blood filled capillaries. Internally, alveoli are lined with a surface tension lowering fluid: pulmonary surfactant, which ensures that alveoli are recruited during breathing. During HFNC therapy, one possible reason positive airway pressure is as significant in treating ARDS is it’s ability to keep alveoli fully inflated and capable of performing gas exchange (39).

The upper respiratory tract includes the nasal and oral airways, as well as the trachea, larynx and pharynx of the upper airways and bronchi in the central airways. Of particular interest to the dynamics of HFNC are the airways extending from the nares to the trachea. This airway is an exceptionally complex geometry with numerous folds, such as the nasal conchae, and local minimum diameters, such as the nasal valve and epiglottis (39). The single airway branches into

two at the nasopharynx, and continues onto the nares (39). Because of its complex geometry, gas flows through this region of the upper airway are especially difficult to model.

### ***Variable Aspects of HFNC delivery***

The most obvious aspect of HFNC delivery influencing its effectiveness is the flowrate delivered. Both clearance and positive airway pressure increase during therapy when HFNC flowrate is increased (23, 24, 26, 29-31, 36). Flowrate however is not the only consideration clinicians must account for when prescribing HFNC, which may influence the other prescribed outcomes. They must also consider the amount of oxygen mixed into the gas, the gas it's mixed in with, cannula sizing, and the specifics of the patients, such as breathing rate and airway size.

Commercial HFNC delivery systems include several cannula, designed to improve patient outcomes and sized to improve comfort. Commercial HFNC are specially designed to best provide therapy, with a special attention to patient comfort. The CFD simulation presented in Miller *et al.* also found that smaller nasal cannula, corresponding to a higher flow velocity, increased the clearance rate from 3.6 s to 2.2 s (33). The same study also found that the selection of a large bore cannula increased the overall pressure compared to a smaller cannula.

One option clinicians have to improve oxygenation is to blend more oxygen into the gas delivered during HFNC therapy. This in turn will change fluid properties, although only slightly. More dramatic changes in fluid properties are possible by using an alternative to air in HFNC. Breathing heliox, a mixture of helium and oxygen, has for example been suggested as a way to reduce resistance during breathing. Heliox has been combined with non-invasive ventilation, and has shown some effectiveness in reducing the need to intubate (40-46). Little research has

been made to date to evaluate the effectiveness HFNC has when combined with gasses other than air and oxygen.

### ***Fluid Mechanics***

During breathing the upper airways remain relatively static, with the airflow of breathing being the result of expansion and contraction of the lung. It follows that flows within the upper airways can be modeled as an internal confined flows, similar to those in a piping system. The geometry of the upper airways makes direct comparison to traditional internal flows challenging. Under normal conditions, flows in and out of the trachea are relatively easily characterized, however this is further complicated by the inclusion of the flows from HFNC (38). While flows in and out of the trachea are controlled primarily by the act of breathing, flows in and out of the nares have a semi-confined jet entering them, adding an additional source of flow.

One of the most important characterizations of a flow is the degree to which the flow is laminar or turbulent. A relatively strong predictor of turbulence in flow is the Reynolds number, written as

$$Re = \frac{\rho ul}{\mu} \quad [1-1]$$

where  $\rho$  is the gas density,  $u$  the flow velocity,  $l$  is the characteristic length, and  $\mu$  is the gas dynamic viscosity. The characteristic length is dependent upon the flow in question, but for internal flows, it is typically some measure of the diameter of the flow passage. The flow transitions from a smooth laminar flow to a turbulent one approximately between Reynolds numbers of  $Re = 2300$  to  $Re = 4000$  for an internal cylindrical flow. Identifying the specific flow velocity and characteristic length that are appropriate for characterizing the flow can pose

a particular problem for such an irregular geometry, and in this case, the transitional Reynolds number may not be the same, due to the irregular geometry in question.

Gas flows in the upper airways during normal tidal breathing are typically on the scale of  $Re \sim 1000$  (47, 48). This places the flow just below the transitional regime, with some local turbulence due to the irregular geometry. During normal breathing, the pressure drop across the airways can be described by the Pedley model (49, 50). While applicable to bronchi and bronchioles, this model cannot be used in the upper airways due to irregular geometry.

Additionally, the nasal airways during HFNC have a time varying flow in the form of breathing, and an additional source of flow in the form of nasal cannula. In order to determine pressure along a streamline, the Bernoulli equation is typically employed, where energy along a streamline is balanced such that

$$P_1 + \rho g z_1 + \frac{\rho}{2} u_1^2 = P_2 + \rho g z_2 + \frac{\rho}{2} u_2^2 \quad [1-2]$$

Where  $P$  represents pressure,  $g$  the force of gravity,  $z$  is elevation and the subscripts 1 and 2 refer to two points along a streamline. Due to the low density of air, and the small size of the upper airways, the changes in elevation can be neglected in this case. This model of flow however does not account for frictional losses of pressure, and relies on both points in question being located on a single streamline. This model can be modified to account for viscous losses in energy along the flowpath such that

$$(P_1 - P_2) = \frac{\rho}{2} (u_2^2 - u_1^2) + RQ^2 + \sum k_i \rho u_i^2 \quad [1-3]$$

Where  $Q$  is the total flowrate,  $R$  is airway resistance between points 1 and 2, and  $k_i$  represents minor loss coefficient at point  $i$ , or energy lost due to individual geometric features of the flow path.

In the case of nasal airways undergoing HFNC, three outlets/inlets of flow must be considered. Those are gas entering via cannula, entering and exiting the trachea due to breathing, and entering and exiting the nares to balance flow. This is illustrated in Figure 1-1. As the air in the nasal airways is approximately incompressible and airway geometry is constant, these three flows must balance at any time during the breathing cycle. During HFNC the flowrate from the cannula is set at a constant value. Consider the pressure developed at the trachea during a pause in the breathing cycle: the flowrate entering through the cannula must be equal to that exiting the nares. Because flow enters and then exits the nares, even if the fluid is static at the trachea, the internal pressure at the point where streamline “turns around” to exit the nares will be the same as that at the trachea, as the remainder of the airway can be considered as approximately static. Losses for flow both entering and exiting the nasal airways must be accounted for, as the pressure at the cannula will increase to maintain a constant flowrate, if resistance to the flow exiting the airway increases.

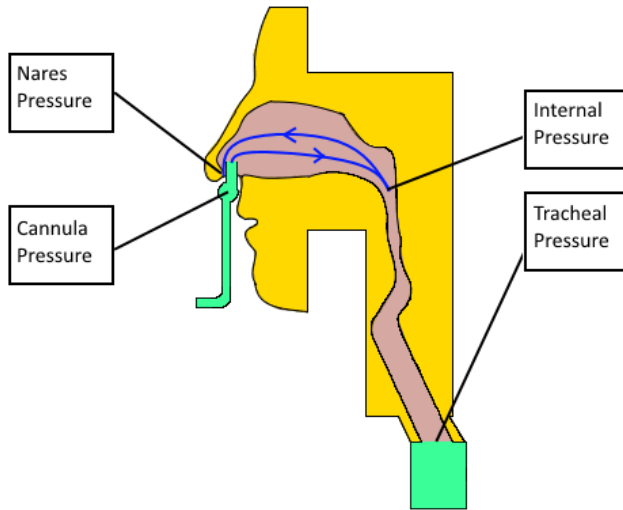


Figure 1-1: A diagram of flows into and out of an upper airway between breaths. Blue arrows represent possible sample streamlines, but are not to be taken as to scale.

Consider the diagram illustrated in Figure 1-1. If the space just outside the nares, the internal pressure are named points 1 and 2 respectively, equation [1-3] can be rewritten as

$$(P_2 - P_1) = \frac{\rho}{2}(u_1^2 - u_2^2) + \sum k_{1-2} \rho u_{1-2}^2 \quad [1-4]$$

Neglecting flow between the trachea and the point at which flow “turns around” inside the airway, the pressure at this internal point will be the same at the trachea during a pause in breathing. As the space outside of the nares is approximately static atmosphere, it can be assumed that there is negligible flow velocity, and that using gauge pressure, the surrounding pressure is  $P_1 = 0$ . Because each airway is different, and the flow pattern will be dynamic during the breathing cycle, the only point at which there is known fluid motion, excluding flow from the trachea during breathing, is out of the cannula and through the nares. The rapid expansion from the nares to the surrounding atmosphere is one minor loss that must be accounted for, which can be written as  $k_{nares\ exit} \rho u_{nares}^2$ . Additionally, there will also be

resistance from the flow exiting against the counterflow exiting the nares. This resistance will be proportional not to the flow velocity of the gas, but the difference between cannula and nares flow velocities, such that a second minor loss can be accounted for as

$k_{counterflow}\rho(u_{nares} - u_{cannula})^2$ , noting the sign of cannula flow to be negative. Combining and rearranging for simplified coefficients, the pressure at the trachea during a pause in breathing can be modeled as

$$P_{internal} = k_{nares}\rho u_{nares}^2 + k_{cannula}\rho u_{cannula}(u_{cannula} - u_{nares}) \quad [1-5]$$

Which leaves only the empirical loss coefficients to be determined. As the cannula velocity is larger than the nares velocity, it follows that the product of the two will be dominated by the square velocity at the cannula. Although this model neglects major losses, because of the inconsistencies in flow pattern, major losses will have to be considered more empirically.

Gas mixing in a semi-confined flow path is a complicated topic. Mixing occurs from a combination of convection (due to fluid motion) and diffusion (due to random motion). With respect to convection, which is often dominant in more dynamic flows, mixing increases with the number and magnitude of turbulent eddies. As progressively smaller eddies begin to form, mixing of two fluid elements increases. This in turn increases with increasing Reynolds number, which is influenced by increasing flow velocity, and increases mixing of exhaled air with fresh gas. The replacement of existing gas in a semiconfined space by jetting poses a challenging question, even without additional sources of motion. Pitts *et al.* investigated the mixing of turbulent axisymmetric jets into semi confined spaces, and found Reynolds number predicted jet unmixedness, finding penetration to increase with  $Re$  (51). Furthermore, as Reynolds

number increases, the distance which a jet can be expected to penetrate into an airway also increases.

Much of the existing *in vitro* experiments relating to fluid mechanics relies on the use of rigid upper airway replicas, including research in HFNC therapy (30, 37, 38, 52-56). During the breathing cycle, the upper airways are not perfectly static. With the exception of conditions such as sleep apnea however, these changes in dimension are minor. For the case of a breathing patient, unsteady effects therefore must be considered. The Strouhal number compares the relative influence of unsteady and convective flows, such that

$$St = \frac{\tau u}{D} = \frac{4\tau Q}{\pi D^3} \quad [1-4]$$

Where  $\tau$  is the time constant for breathing inhalation, and  $D$  is the airway diameter. Typically for large Strouhal numbers, unsteady components of flow can be ignored and average convective components dominate. A typical tidal breathing pattern with a tidal volume of 500 mL and frequency of 18 breaths/min, with inhalation half that of exhalation, would result in average inhalation flowrates of  $Q = 27$  L/min, over the course of  $\tau = 1.11$  s. The Finlay lung model recommends a diameter of  $D = 1.81$  cm at the trachea (38). In this case, the Strouhal number is  $St = 107$ , which is sufficiently large to determine that convective effects dominate unsteady effects in the upper airways.

### **Purpose of Research**

It is the objective of this thesis to investigate how HFNC affects the upper airway clearance of exhaled air, as well as the positive airway pressure resulting from the therapy. The *in-vitro* experiments presented here attempt to do that, by providing HFNC therapy to physiologically accurate upper airway replicas. Of particular interest are the design of cannula, HFNC flowrate,

breathing pattern and gas delivered during therapy to a particular airway geometry. Due to the relative nascence of HFNC, guidelines on use of the therapy are lacking. Some clinicians remain unsure of the degree to which certain changes in HFNC, such as increasing flowrate, or switching patients to a low-density gas will affect outcomes. By clearly linking changes in HFNC delivery to the degree of upper airway deadspace clearance, and positive pressure, clinicians will be better equipped to respond to changes in during therapy.

### **Thesis Structure**

This thesis is presented in mixed-format of published and under review research. The first chapter presents an overview of existing literature in the field of HFNC therapy. This ranges from clinical uses of therapy to specifics of its mechanisms of action. Also presented here is a background in the basic fluid sciences which will inform later experimental research. The second chapter, currently in circulation in the journal *Clinical Biomechanics*, analyses HFNC use in adult upper airway replicas. Using a non-breathing model, upper airway clearance time was measured and compared with changes in cannula size and HFNC flowrate. Using a breathing model, pressure was also compared with cannula size and HFNC flowrate. The third chapter, currently under review, compares both upper airway clearance and positive airway pressure in breathing upper airway replicas, while accounting for the influence of gas density. The fourth and final chapter summarizes results of the second and third chapters, and presents possible future venues for research.

## **Chapter 2 Correlation of High Flow Nasal Cannula Outlet Area and Flow with Non-Breathing Gas Clearance and Positive Pressure in Adult Upper Airway**

### **Replicas**

A very similar version of this chapter has been published as: Moore, C. P., Katz, I. M., Caillibotte, G., Finlay, W. H., Martin, A. R. (2017) "Correlation of high flow nasal cannula outlet area with gas clearance and pressure in adult upper airway replicas" *Clinical Biomechanics*, DOI: 10.1016/j.clinbiomech.2017.11.003

### **Introduction**

Acute respiratory failure is a cause of approximately 30% of ICU admissions, and symptoms may persist despite treatment (57). Origins of such respiratory failure are numerous; acute lung injury (ALI) or acute respiratory distress syndrome (ARDS), related to community- and hospital-acquired pneumonias, sepsis, chest or head injury, aspiration, or other causes, can rapidly progress to acute respiratory failure requiring noninvasive or invasive mechanical ventilation (7, 13, 58) .

An increasingly common intervention for acute respiratory failure is the use of high flow nasal cannula (HFNC) therapy to support patient breathing (7, 13, 59-62). HFNC delivers heated and humidified mixtures of oxygen and air through specialized nasal cannulas (59). HFNC typically delivers gas at up to 60 liters per minute (LPM), although higher flow rates, up to 100 LPM, have been investigated (31). Oxygen provided by HFNC has been shown to improve oxygenation and reduce ventilation requirements in critical care subjects (59). In a recent large, randomized clinical trial enrolling patients with non-hypercapnic acute hypoxemic respiratory

failure, HFNC oxygen therapy resulted in reduced mortality in the ICU and at 90 days, as compared with standard oxygen therapy or noninvasive ventilation (13).

While data for hypoxemic patients using HFNC is promising, existing reports do not conclusively characterize the underlying mechanisms of action, especially for patients on palliative care, or at risk of respiratory failure due to muscle fatigue (63, 64). Delivery of high flows in excess of patient inspiratory flow rates allows the fraction of inhaled oxygen ( $FiO_2$ ) to be tightly controlled by adjusting the oxygen concentration in the delivered gas mixture. Additionally, the provision of high flow incurs a small positive distending pressure, which may improve ventilatory mechanics and maintain alveolar patency similar to the maintenance of continuous positive airway pressure (CPAP) (1). However, computational fluid dynamics (CFD) simulations suggest pressures equivalent to those of continuous positive airway pressure (CPAP) above 6 cmH<sub>2</sub>O are not typical (37).

Another primary benefit that is proposed of HFNC is the ability to washout exhaled carbon dioxide (CO<sub>2</sub>) from the nasal cavity, such that a higher concentration of oxygen can be inspired, especially during weak or injured breathing (1, 37). For this mechanism, the nasopharyngeal dead space becomes a reservoir for fresh gas, which ensures that during the beginning of inspiration the inhaled oxygen volume is maximized, while washing out CO<sub>2</sub>, thus increasing alveolar efficiency. It has been suggested that a primary advantage of HFNC therapy over conventional CPAP is this continuous washout, or dead space clearance, mechanism (1).

The nasopharyngeal space is a complex geometry, making dead space clearance challenging to model analytically. Experimental results reported by Moller et al. in a static, geometrically realistic nasopharyngeal replica indicated that the use of high flow has the capacity to increase

the rate at which dead space gas is replaced (65), for therapy flows of up to 45 LPM. As the flow rate received from the cannula increased from 15 to 45 LPM, a statistically significant decrease in clearance half times was measured (65). Similarly, Van Hove et al. (37) experimentally evaluated CO<sub>2</sub> clearance in a realistic nasal cavity replica to confirm CFD simulations done in the same geometry, concluding that CO<sub>2</sub> clearance increased with delivered flow rates up to 60 LPM. Previously, studies of aerosol deposition during HFNC have demonstrated significant backflow through the nasal passages, which may indicate increased clearance (66, 67). Additionally, Gardner et al. (68) demonstrated experimentally CO<sub>2</sub> clearance of upper airways in accurate replicas of infant upper airways.

In the present study, we examined the influence of HFNC flow rate on clearance times and tracheal pressures *in vitro* in five adult nasal airway replicas. Use of multiple geometries permitted insight into intersubject variability in gas clearance and airway pressure arising from variation in nasopharyngeal geometry. In addition, the potential influence of nasal cannula size was investigated by repeating experiments for two HFNC used with commercial high flow delivery systems, and a standard cannula commonly used for low-flow oxygen administration.

## Methods

### *Nasal Airway Replicas*



*Figure 2-1: Side and front view of upper airway replica. Specific replica shown corresponds to "Subject 2".*

Nasal airway replicas were constructed in acrylic using rapid prototyping (Invision SR 3-D printer) based on magnetic resonance imaging (MRI) scans of healthy adult subjects as described elsewhere (69). The subjects were originally selected in Golshahi et al. (2011) from a larger set of subjects to represent a wide range of pressure drops from the nares to the trachea of the replicas (69). The nasopharynx and larynx were constructed separately and then joined with screws and sealing glue to form the complete model (69). Oral airways were not included in the replicas. This reflects the closed-mouth condition, where distending pressure effects have been shown to be greatest (70). Demographic and geometric parameters for the replicas are listed in Table 2-1. Subject volume, surface area and path length are described in Golshahi et al. (2011), and nares areas of the printed replicas were measured using precision calipers to

measure diameters, and approximated as elliptical. The replica of Subject 2 is shown in Figure 2-1. Replicas included the face and airways from the nares to the trachea. Inclusion of the face allowed a natural placement of the cannula in the replica nares. Nonetheless, cannulas were removed and repositioned before each experimental replicate, in order to capture uncertainty in prong positioning within the nares. Cannula were inserted fully into the nares, allowing the base of the cannula to touch the columella.

*Table 2-1: Rapid prototyped upper airway replica subject parameters. Data from Golshahi et al. (69)*

<b>Subject</b>	<b>Sex</b>	<b>Airway Volume, V (mm<sup>3</sup>)</b>	<b>Nares to Trachea Length, L (mm)</b>	<b>Internal Surface Area, A<sub>s</sub> (mm<sup>2</sup>)</b>	<b>Nares Opening Area, A<sub>n</sub> (mm<sup>2</sup>)</b>	<b>Average Airway Cross Sectional Area, A<sub>c</sub>=V/L (mm<sup>2</sup>)</b>
2	F	44567	241	28718	63.8	185
5	F	35859	210	23532	89.2	171
6	M	50125	269	31345	89.0	186
8	M	47264	223	28936	82.2	212
9	M	45267	239	25086	103.5	189

### **Gas Clearance Measurements**

For gas clearance measurements, dry oxygen at room temperature was supplied to the cannula from a regulated cylinder (Praxair Canada, Edmonton, AB Canada). The flow rate of oxygen to the cannula was controlled by a mass flow controller (MCR-100SLPM-D/5M, ALICAT Inc., AZ USA) to allow variability in flow rate provided. Flow rates of 30, 60 and 90 standard LPM were tested to include the extreme range of clinical flows (31). Although humidified gases are supplied during HFNC therapy in the clinical settings, the changes in viscosity, density and diffusivity between dry room temperature air and oxygen, and humidified 37 °C air and oxygen are less than 10%, and will have a minimal effect on clearance trends.

Transport within adult upper airways is dominated by advection over diffusion (71), such that measurement of oxygen wash-in correlates directly with air wash out. Furthermore, wash-in of oxygen during HFNC therapy is a key function of the therapy when supply oxygen rich gas to patients (72). In the present experiments, clearance of air from the nasal airway replicas was determined by measuring the increase in oxygen concentration over time.

The oxygen concentration was sampled at a rate of 34.5 Hz at the trachea and larynx of the model using a laser diode gas analyzer (GA-200; iWorx Systems Inc., NH USA, accurate to 0.01%). Tracheal oxygen concentration was monitored by placing a standard breathing circuit gas sampling adapter at the exit of the replica. This arrangement positioned the entrance to the sample line 1 cm downstream from the exit of the replica. Oxygen concentration in the larynx was monitored by inserting the sample line at the distal exit and placing the sampling port approximately 8 cm proximal to the exit of the replica, using sample line length as the point of reference. A diagram of the system is shown in Figure 2-2. Between tests, atmospheric air was drawn into the replica to return oxygen content to 21%. During testing, the replica was plugged at the trachea, such that tests represent replacement of air with oxygen during a breath hold.

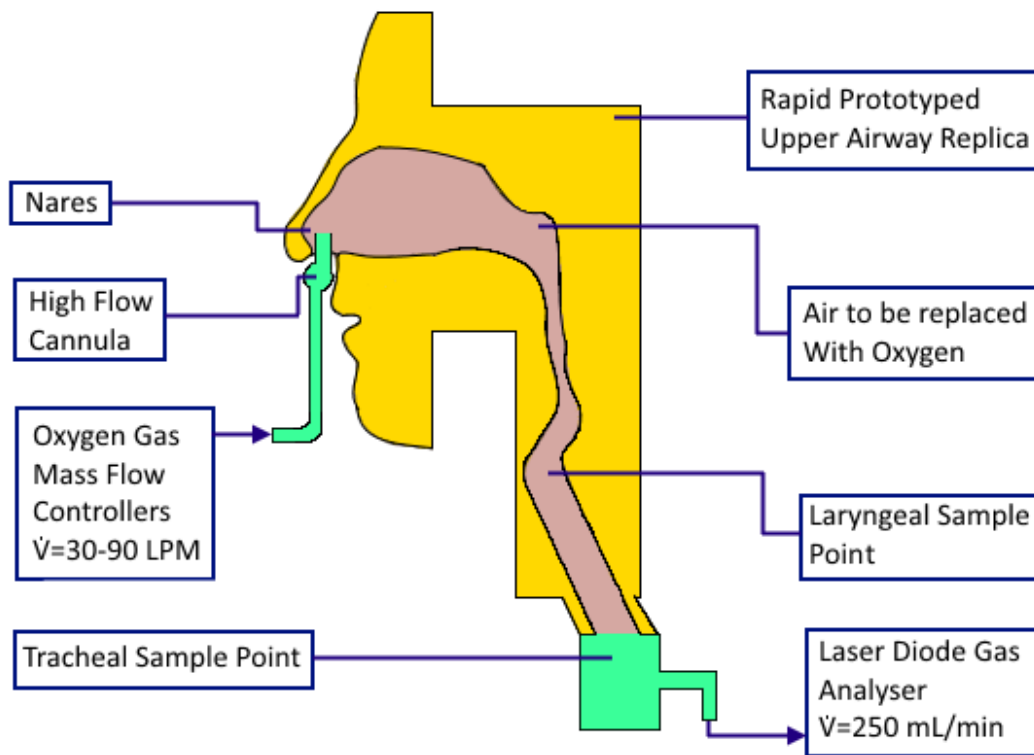


*Figure 2-2: A diagram of the dead space clearance model. Oxygen is supplied from the HFNC gas supply, which replaces the air normally within the airway replica. The gas analyzer sample line is placed at the exit of the model, located at the trachea, or within the model at the larynx.*

A sampling flow rate of 250 ml/min was used throughout. Sampling flow rates of 100 ml/min, 250 ml/min and 400 ml/min were compared in preliminary tests when supplying 30 SLPM of oxygen through a straight commercial cannula. While 400 ml/min was found to affect the measured rate of clearance, the difference in clearance times between 100 ml/min and 250 ml/min sample was negligible for times to achieve 50%, 75% and 95% oxygen (Student's t-test,  $p > 0.05$ ).

Data from the gas analyzer was collected using a custom data acquisition program (Labview; National Instruments, TX USA). The time expended between 25%, 50%, 75% and 95% oxygen

concentration in sampled gases was determined using a custom Matlab® (Mathworks, Natick, MA USA) code to analyze the text file outputs. The start time coinciding with 25% oxygen was chosen so as to avoid false starts as baseline oxygen concentration fluctuated occasionally above 21% due to noise. Clearance time measurements were repeated five times for each combination of airway replica, flow rate and cannula.



*Figure 2-3: Cannula used in testing. Shown are large (top), medium (middle) and small (bottom) cannula.*

Three commercial cannulas were tested in order to explore a range of cannula sizes, shown in Figure 2-3. Two of these cannula are designed for use with high flow therapy (Adult Cannula; Vapotherm®, Exeter NH USA), (Optiflow™ 5-series size L; Fisher & Paykel®, Auckland New

Zealand), and the third is a generic straight cannula (Adult Nasal Cannula 1104; Teleflex Medical Inc., NC USA). The outlet diameters, corresponding to the inner diameter, of the cannula prongs were measured and used to calculate areas, which are displayed along with the Reynolds number of the oxygen flow in Table 2-2. Outlet areas were used to determine the Reynolds number exiting the cannula. Outlet areas were assumed to be elliptical and the area was determined by measuring minimum and maximum diameter. The Reynolds number is calculated as:

$$Re = \frac{2\left(\frac{\dot{V}}{A}\right)\sqrt{\frac{A}{\pi}}}{\nu} \quad [2-1]$$

where  $A$  is the area of the cannula outlet estimated by measuring the inner diameter and approximating the area to an ellipse,  $\dot{V}$  is the volumetric flow rate and  $\nu$  the gas kinematic viscosity. Cannula outlet areas were approximated as circular for simplicity (the use of an elliptical length scale in the Reynolds number gave negligible changes to the results).

Volumetric flow was set by the mass flow controller, calibrated to pure oxygen. Here the viscosity for oxygen for standard atmospheric temperature and pressure is  $\nu = 1.4 * 10^{-5} \text{ m}^2/\text{s}$ .

*Table 2-2: Cannula outlet area, corresponding to the cannula inner diameter, cannula prong outer area, corresponding to the cannula outer diameter, and Reynolds number at tested flow rates exiting the cannula outlet.*

<b>Cannula</b>	<b>Optiflow size L (Large)</b>	<b>Generic Straight (Medium)</b>	<b>Vapotherm Adult (Small)</b>
<i>Cannula outlet area, <math>A_i</math> (<math>\text{mm}^2</math>)</i>	21.65	9.62	7.07
<i>Cannula outer area, <math>A_o</math> (<math>\text{mm}^2</math>)</i>	25.13	15.90	14.52
<i>Reynolds Number at 30SLPM</i>	8.66E+03	1.30E+04	1.52E+04
<i>Reynolds Number at 60SLPM</i>	1.73E+04	2.60E+04	3.03E+04
<i>Reynolds Number at 90 SLPM</i>	2.60E+04	3.90E+04	4.83E+04

### ***Distending Pressure Measurements***

In order to determine distending pressures resulting from nasal high flow therapy, airway replicas were connected at the outlet through a short length of standard 22 mm diameter breathing circuit tubing to a mechanical lung simulator (ASL5000; Ingmar Medical Inc., Pittsburgh PA USA). Data was sampled at a rate of 500 Hz to a precision of 0.001 cmH<sub>2</sub>O. A sinusoidal breathing pattern was imposed, with a tidal volume of 500 ml at a breathing frequency of 18 min<sup>-1</sup>, chosen to be comparable with Chanques et al.(25) Real-time pressure and volume data was recorded by the lung simulator for 5 successive breaths. The pressure recorded is essentially equal to that averaged over the replica outlet (i.e. the trachea), as the tubing connecting the replica to the lung simulator produced negligible frictional pressure losses, estimated to be less than 0.04 cmH<sub>2</sub>O, or 1% of pressure amplitude throughout the flow breathing cycle when no oxygen is supplied. As such, the pressure reading from the lung simulator is here referred to as tracheal. Airflow was provided from a house compressed air line, through the nasal cannula at rates of 0, 30 and 60 LPM using the three commercial cannulas described above, with flow controlled using a mass flow controller (MCR-100SLPM-D/5M, ALICAT Inc., AZ USA). The 90 LPM flow was omitted from the pressure measurements due to high tracheal pressures observed at 60 LPM flows. Three repetitions for each test were performed.

Pressure waveform data was output by the lung simulator, and a script written in MATLAB<sup>®</sup> was used to extract the maximum, minimum, and mean pressures for each breath, as well as the positive end expiratory pressure (PEEP), defined as detected airway pressure at end of expiration cycle (no breathing flow).

### ***Statistical Methods***

In order to determine significance of trends, 3-factor ANOVA was performed on oxygen content sampled at the larynx and trachea, and tracheal pressure during tidal breathing. Post-hoc analysis was performed to isolate and compare the influence of cannula selection and flow rate. Tukey HSD post hoc was used as the primary statistical analysis. Multi-variable linear regression was performed to test tracheal pressure dependence on flow, cannula and subject variables. All statistical analysis was performed in the SPSS environment (IBM SPSS; IBM Corp., NY USA).

### **Results**

#### ***Clearance Time***

Average tracheal and laryngeal clearance times for the five replicas are shown in Figure 2-4. Clearance time is defined as the time measured between 25% and 50%, 75% or 95% oxygen at the sample point. Clearance time decreases from the larger to the smaller cannula for all flow rates and at both the trachea and the larynx. Additionally Figure 2-4 shows that as oxygen flow rate increases, the clearance time decreases. This trend is consistent with the theory for fully mixed volumes where the time constant for wash-in is the quotient of container volume, and volume flow (65).

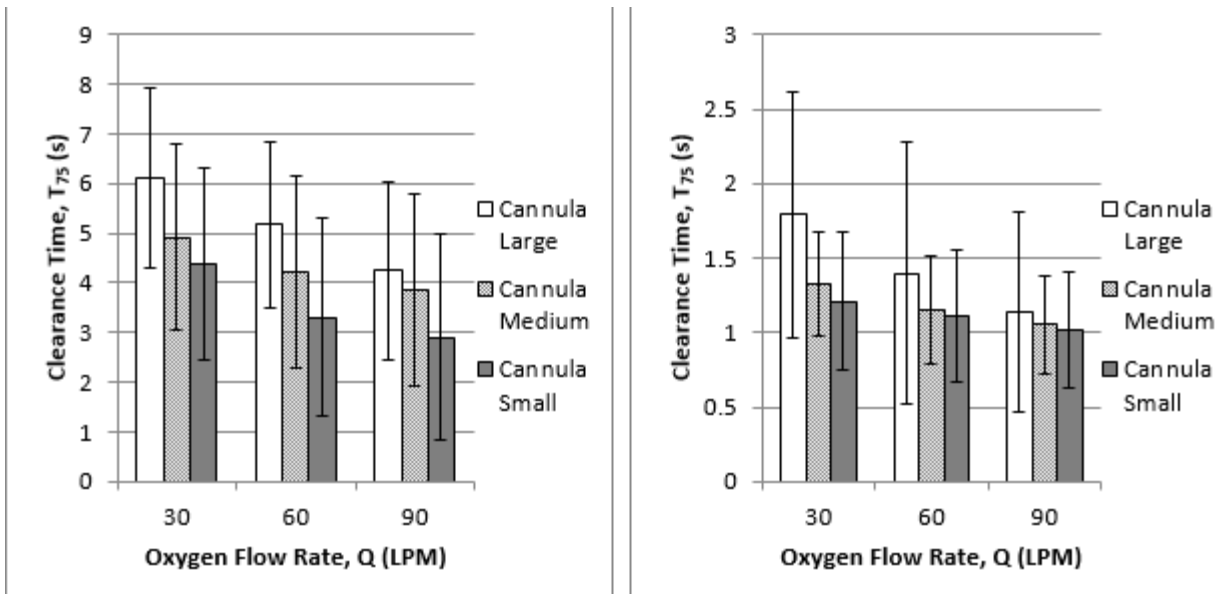


Figure 2-4: Average clearance times of all subjects, from 25% to 75% oxygen, sampled at the trachea (left) and larynx (right). Error bars represent the propagated standard deviations of the subject means ( $n=5$ ).

The influence of subject, flow rate and cannula on clearance times are all statistically significant ( $P<0.001$ ). Two and three variable interaction was also present ( $P<0.05$ ) in all cases except in the case of tracheal measurements of 25%-50% oxygen ( $0.15<P<0.48$ ), implying the 3 factors cannot be accurately assessed in isolation. The results of the post-hoc test for clearance time between 25%-50%, 25%-75% and 25%-95% oxygen at both the trachea and larynx confirm ( $P<0.01$ ) that the clearance times were slower for the largest cannula than for the two smaller cannulas. Further, the small cannula resulted in faster clearance times than the medium cannula ( $P<0.01$ ) for the tracheal measurements; however, the difference was not statistically significant ( $0.095<P<0.401$ ) in the case of laryngeal sampling.

## Distending Pressure

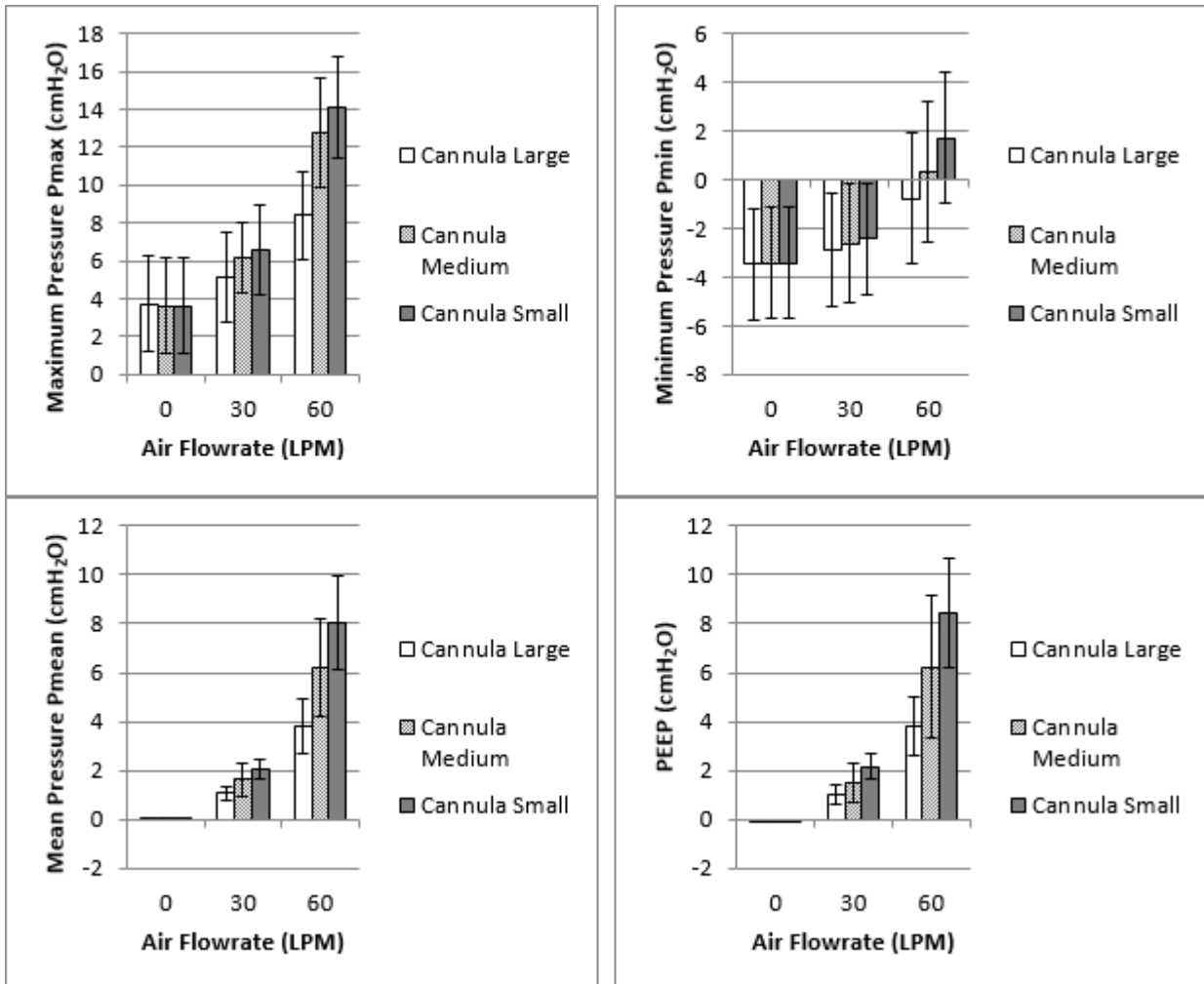


Figure 2-5: Average pressures of 5 subjects ( $n=3$ ), measured at cycle maximum (top, left), cycle minimum (top, right), cycle mean (bottom, left) and positive end of expiration pressure (PEEP) (bottom, right). Pressures extracted from pressure waveform over 5 breaths measured by the mechanical lung to approximate tracheal pressure in breathing subjects. Error bars represent the propagated standard deviations of the subject means ( $n=5$ ). Note:  $1 \text{ cmH}_2\text{O} = 98.07 \text{ Pa}$ .

The average pressures for the three cannulas in the five airway replicas are presented in Figure 2-5. Pressures are gauge values compared to the atmosphere. For all four pressure

parameters displayed in Figure 2-5, there was a significant effect of cannula selection, subject selection, and flowrate ( $P < 0.001$ ). Additionally, simple factor interaction was also present between the three independent variables ( $P < 0.001$ ). Post hoc analysis showed in all cases an increase in pressure from large to medium to small cannula ( $P < 0.001$ ), as well as the expected increase in pressure with increasing cannula flow rate ( $P < 0.001$ ).

## **Discussion**

### ***Cannula Clearance Performance***

Cannula selection is a major factor in determining clearance time. Average clearance times, shown in Figure 2-4, show that the small cannula consistently has shorter clearance times than the larger cannulas.

The effect of both supply flow rate and cannula outlet diameter on clearance time is captured by the Reynolds number, as  $Re \propto \dot{V}/d$ . The clearance time is plotted as a function of Reynolds number for each replica in Figure 2-6, where gas properties correspond to 100% oxygen. For a given replica geometry, clearance time is seen to decrease with increasing Reynolds number. This corresponds with a decrease in cannula diameter or an increase in supplied flow rate. The correlation shown however is not consistently strong for all replicas studied, ranging from  $R^2 = 0.20$  to  $R^2 = 0.94$ . This intersubject variability likely reflects the lack of subject geometric factors in our definition of the Reynolds number. Although mixing increases with turbulence, it is likely that because this is not a simple geometry, other considerations beyond Reynolds number and turbulence have a significant influence.

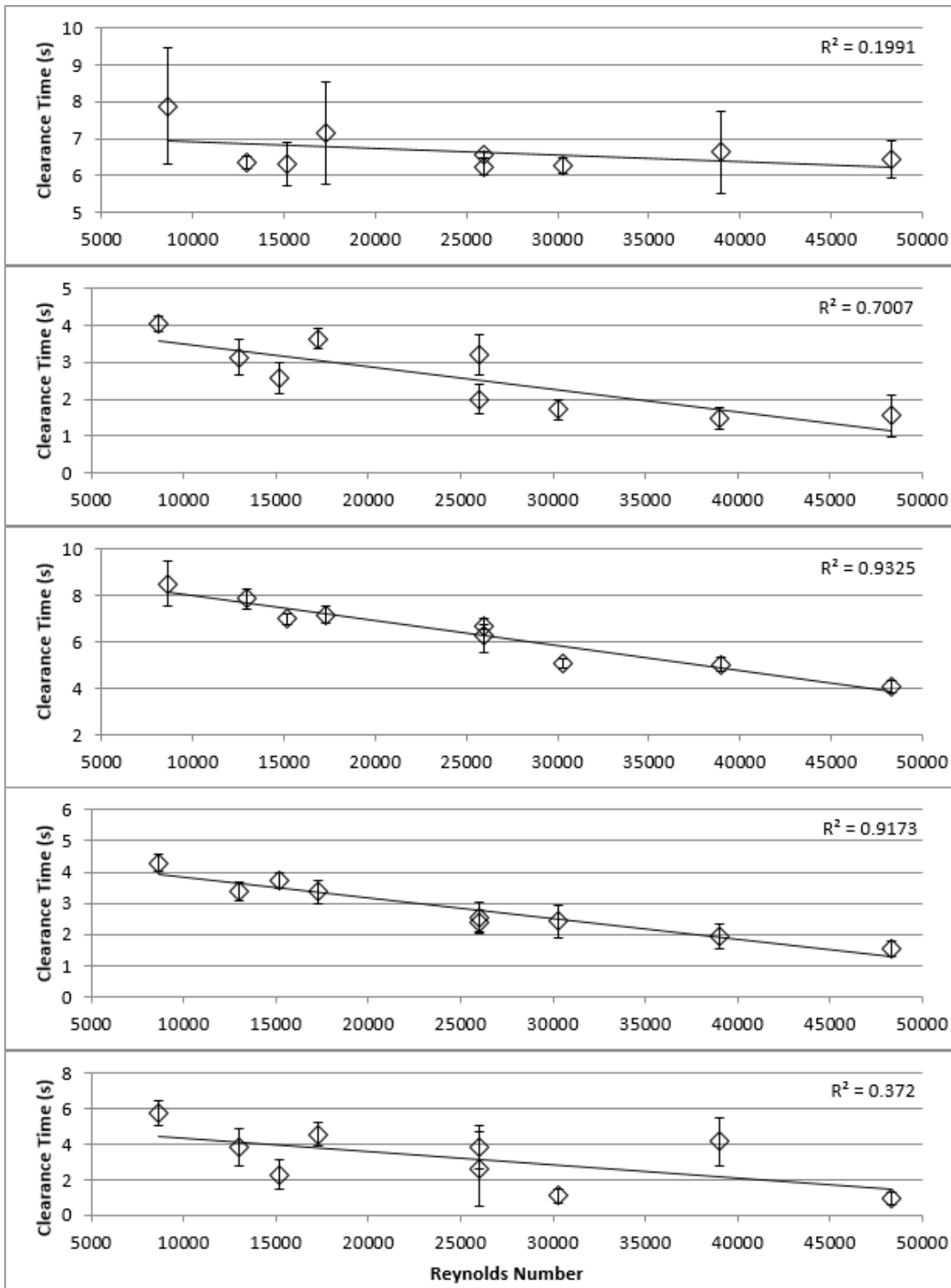


Figure 2-6: Clearance time as a function of Re measured at the subject cannula. Panels in descending order correspond to subject 2, 5, 6, 8 and 9. Reynolds number determined as described in Equation (2-1). Error bars represent 1 standard deviation for test point (n=5).

While geometric effects, such as the curvature of cannula, may influence clearance times, given the strong influence of cannula outlet area, the exit velocity is likely the dominant governing flow field parameter. This is supported by the Reynolds number dependence seen in Figure 2-6. The Reynolds number is a measure of the importance of fluid inertia compared with viscous effects in determining momentum transport. Based on the Reynolds numbers exiting the cannula, ( $Re > 4000$ ) the flow exiting the cannula can be expected to be turbulent and dominated by inertial effects. As the flow is directed into an enclosed space, the penetrating depth of the oxygen flow will be dictated by its exit momentum. Thus, all else being equal, higher velocities of oxygen flowing into the nasal geometry can be expected to give faster clearance. This conclusion is supported by Miller et al. (2016) where computational simulations of HFNC showed that purging of upper airway increases with the greater flow energy resulting from higher velocity gas exiting the cannula (73). In addition to these simple momentum considerations, higher jet velocities exiting the cannula can be expected to produce higher shear at the edge of the jet, increasing turbulent mixing (74), again leading to faster clearance. This turbulent mixing may also explain the decreased clearance time experienced at the larynx. As flow velocity increases, the intensity and convective penetration of the turbulence increases as well. As the larynx is proximal to the trachea, the larynx can be expected to be exposed to more turbulent mixing and thus faster clearance.

It has been previously hypothesized that the wider cannula bore of some specialized HFNC improves their performance by avoiding discomfort due to high airflow velocity, or jetting (1). However, this approach to increasing comfort could decrease effectiveness. Indeed, the model with the largest exit cross section consistently has the longest clearance time. Conversely,

smaller exit cross sectioned cannula achieved shorter clearance times, implying increased clearance rate with flow velocity exiting the cannula.

### ***Cannula Distending Pressure***

Minimum, maximum and mean tracheal pressures for the Optiflow™ cannula were reported previously in Chanques et al.(25), where clinical patients with tracheostomies underwent high flow oxygen therapy (HFOT) while breathing normally, and pressure was measured through the tracheostomy. The tracheal pressures found by Chanques et al.(25) are in reasonable agreement with those measured in the replicas and shown in Figure 2-5. For example, Chanques et al. (16) report a 25-75<sup>th</sup> percentile range of mean pressures of 1.3 to 2.5 cm H<sub>2</sub>O (130 to 245 Pa) for Optiflow™ cannula supplied with 30 LPM, where cannula size was selected according to patient nostril size. The mean pressure measured *in vitro* in the present study for 30 LPM flow supplied through the Optiflow™ size L cannula was 1.06 cm H<sub>2</sub>O, with a standard deviation of 0.31 cm H<sub>2</sub>O (104 ± 30 Pa). Thus, the *in vitro* model employed here appears to reasonably approximate the pressures measured *in vivo*.

While there is intersubject variability in tracheal pressures in the present study, reflected by the error bars seen in Figure 2-5, there is no significant difference in pressure resulting from cannula selection at 0 LPM flow, even when controlling for subject geometry. This suggests that the extent of occlusion of the airways by the cannula has little effect on the pressure differences measured. The differences between cannula performances at higher flow rates are likely due instead to the higher flow velocity provided by the smaller cannulas.

These trends of increasing tracheal pressure with increased flow velocity at the cannula outlet may in part reflect pressure and flow changes described by a mechanical energy balance,

$$P_1 + \frac{1}{2}\rho v_1^2 = P_2 + \frac{1}{2}\rho v_2^2 + H \quad [2-2]$$

where  $P$  represents the pressure at a point along a flow streamline (point 1 or 2),  $v$  the flow velocity,  $\rho$  is the density and  $H$  represents frictional pressure losses between points 1 and 2 (where gravity has been neglected). Equation (2-2) describes a balance between pressure and kinetic energy. By forcing the oxygen flow through a smaller area and thus at a greater velocity, the flow enters at a larger kinetic energy that can be converted into pressure downstream.

In addition, during HFNC therapy, flow exits the nasal airways through the annular space between a subject's nares and the outer cannula prong walls (determined by measuring the maximum and minimum diameters of the nares, and approximating the area to an ellipse, subtracting the cannula occlusion). This space represents an area constriction, or pinch point, that may contribute significant energy losses,  $H$  in equation (2-2). Such losses generally correlate with the square of the local flow velocity. Accordingly, an attempt was made to correlate measured PEEP values with the squares of velocities exiting the cannula outlet and through the constriction at the nares:

$$PEEP \cong C_1\rho v_{cannula}^2 + C_2\rho v_{nares}^2 + C_3 \quad [2-3]$$

Where  $C_1$ ,  $C_2$  and  $C_3$  are constants and for air at standard temperature and pressure,  $\rho \cong 1.225 \text{ kg/m}^3$

Assuming there is a pause in breathing at the end of expiration, and treating air as incompressible, mass flow balance dictates that the flow rate through the cannula is exactly equal and opposite to that exiting through the nares at the moment PEEP is measured, and the

above equation can be rewritten as

$$PEEP \cong C_1 \rho \left( \frac{\dot{V}}{A_{cannula}} \right)^2 + C_2 \rho \left( \frac{\dot{V}}{A_{nares,open}} \right)^2 + C_3 \quad [2-4]$$

The open nares area is determined as the nares area unoccluded by cannula. The total nares areas (for both nares combined) are listed in Table 2-1.

$$A_{nares,open} = A_n - A_{cannula} \quad [2-5]$$

Multiple regression of PEEP measured for all replicas following the format of eqn. (4) results in an adjusted Pearson's squared coefficient of  $R^2 = 0.906$ , where

$$PEEP \cong 0.026\rho \left( \frac{\dot{V}}{A_{cannula}} \right)^2 + 1.462\rho \left( \frac{\dot{V}}{A_{nares,open}} \right)^2 + 5.549 \text{ Pa} \quad [2-6]$$

The predicted PEEP is compared directly to that measured in Figure 2-7. While the value of  $C_1$  is small relative to  $C_2$ , both are significant (2-factor regression,  $P < 0.001$ ). Despite the smaller coefficient, the influence of flow exiting the cannula is greater than that exiting through the nares, as the squared velocity at the cannula is much greater than that exiting the nares. Note that in equation (2-4)  $C_1$  and  $C_2$  are unitless and PEEP is given in Pa.

The strong predictive capability of eqn. (2-6) supports the notion that flow velocity exiting the cannula and out of the nares are the primary parameters of importance in determining cannula performance. Outliers can be seen in Figure 2-7, and appear to increase in magnitude with the predicted PEEP. This may reflect unaccounted factors influencing PEEP, such as regions of flow separation unique to each geometry.

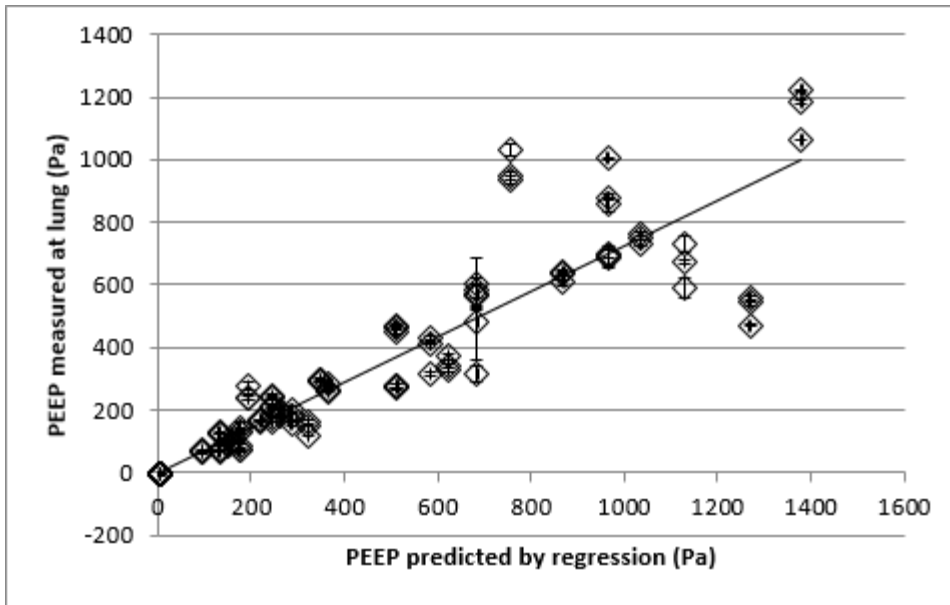


Figure 2-7: A comparison of measured PEEP and PEEP predicted by equation (2-6). Error bars represent 1 standard deviation of PEEP measured at the trachea (n=3)

The pressure measured at the trachea increases both with an increase in cannula flow velocity and an increase in nares flow velocity (see equation (2-6)). For the cannula designs and sizes included in this study, the velocity exiting the cannula dominated; however, should the cannula prong size increase relative to the size of a subject's nares, the velocity at the nares may become increasingly significant.

In order to maximize upper airway pressure, it may be possible to increase flow velocity at both the cannula and the nares by having thick-walled cannula prongs with narrow inner diameters. Increasing cannula wall thickness however may increase clearance times, as it is likely that minimal nasal occlusion leads to an increased rate of gas clearance. As such, greater cannula wall thickness may increase tracheal pressure at the expense of reduced clearance times.

### ***Study Limitations***

Several limitations to our *in vitro* study design can be noted. First, gas clearance experiments were conducted without simulating cyclic breathing through the airway replicas. Therefore, no conclusion can be drawn regarding the influence of breathing parameters (e.g. tidal volume, breath frequency) on clearance rates. Addition of simulated breathing would be expected to increase clearance rates (65). Results presented above should therefore be interpreted as indicating relative differences in static clearance rates between nasal cannulas and at different flow rates, but not predictive of absolute clearance rates with breathing included.

Second, use of rigid airway replicas in both the clearance and pressure experiments ignores any potential influence of high flow therapy on upper airway geometry. Such influence might be particularly relevant for HFNC therapy used to treat patients with upper airway collapse, as in obstructive sleep apnea. The potential for HFNC therapy to alleviate upper airway obstruction is not evaluated here (18). Likewise, the present study did not evaluate the influence of mouth position (open or closed), or position of the soft palate and vocal cords, on clearance rates or pressures generated during HFNC therapy.

Finally, while the present study employed adult airway replicas, inclusion of child and infant airways could allow for more generalized predictions with respect to effects of high flow nasal cannula design on clearance rate and airway pressure.

### **Conclusions**

Both upper airway clearance rate and tracheal pressure increased with flow rate in our high flow therapy measurements. The clearance rate and tracheal pressure also increased with

decreasing cannula outlet diameter. The dependence upon outlet velocity and nares velocity of tracheal pressure follows that expected from a mechanical energy balance. As both increased flow rate and tracheal pressure are generally associated with improved clinical outcomes, it may be that a smaller cannula outlet could be used to improve these outcomes.

## Chapter 3 High Flow Nasal Cannula: Influence of Gas Type and Flow Rate on Airway

### Pressure and CO<sub>2</sub> Clearance in Adult Nasal Airway Replicas

A very similar version of this chapter is at the time of writing under review for publication. The authors listed are: Moore, C. P., Katz, I. M., Pichelin, M., Caillibotte, G., Finlay, W. H. and Martin, A. R.

#### Introduction

High flow nasal cannula (HFNC) therapy is a form of non-invasive respiratory support that has been used to treat respiratory failure in adults (1, 2, 72). The therapy uses heated and humidified gas, delivered through specialized nasal cannula to patients at high flow rates. Gas flows typically range in adults from 15-60 LPM, although higher flowrates have been considered (31, 59). In adults, HFNC therapy is often used to treat a variety of respiratory disorders, such as acute respiratory failure in chronic obstructive pulmonary disorder (COPD) (1, 2, 75). When compared to conventional oxygen therapy, HFNC has shown reduced reintubation and improved secondary outcomes, and similar outcomes to other forms of respiratory support, such as non-invasive ventilation, in post-extubated patients (14, 72, 75-77).

One of the primary mechanisms of action of HFNC, which distinguishes it from other forms of respiratory support, is the upper airway washout effect (1, 2). As HFNC uses an open interface, the gas flowing from the cannula displaces exhaled air from the upper airway, thereby increasing the volume of oxygen and decreasing the amount of CO<sub>2</sub> re-inhaled. *In vitro* and *in silico* studies investigating the upper airway washout effect have found CO<sub>2</sub> clearance increases with flow rate, although this increase is less pronounced at higher flow rates (30, 37, 78). Recent *in vitro* experiments done in realistic adult nasal airway replicas found that faster

gas clearance corresponded with higher flow rates and with smaller cannula outlet area (33, 78).

A second mechanism of action widely attributed to HFNC therapy is in the potential to deliver positive distending pressure at the upper airway. HFNC has been reported to offer a pressure similar to that of continuous positive airway pressure therapy (CPAP) (1, 2). Positive distending pressure has been associated with positive outcomes for many respiratory disorders, most notably during acute respiratory failure (2). Several correlations for the level of positive pressure and flow rate during HFNC therapy have been suggested (26), and there exists evidence that the pressure at the trachea increases quadratically with HFNC flow rate (30, 78). Based on a mechanical energy balance, Moore *et al.* proposed an empirical relationship for predicting positive end expiratory pressure (PEEP) at the trachea as a function of the squares of average flow velocities exiting the cannula and exiting the nasal airway through the nares (78).

Due to their lower flow resistance, it has been hypothesized that the administration of low density gases, such as helium-oxygen mixtures (heliox), improves oxygenation and reduces work of breathing (79, 80). One study of infants with acute bronchiolitis undergoing HFNC therapy found significant improvement in blood oxygenation when using helium-oxygen mixtures compared with air/oxygen (81). Although many studies have investigated the influence of heliox on the effectiveness of respiratory support during invasive and non-invasive ventilation (40-46), little work has been done to examine how gas properties affect pressure and clearance in the upper airways during HFNC therapy.

In the present study, an *in vitro* experimental model was developed to test the effects of gas delivery using HFNC on upper airway pressure and gas washout. Flow rates were varied across a

range typically used to treat adults experiencing respiratory failure. Experiments were conducted for three different gases: air, oxygen and a mixture of helium and oxygen. Three cannula sizes were evaluated. Five realistic adult nasal airway geometries were used, to provide insight into intersubject variation in airway pressure and washout resulting from variation in airway geometry.

## Methods

### Experimental Setup

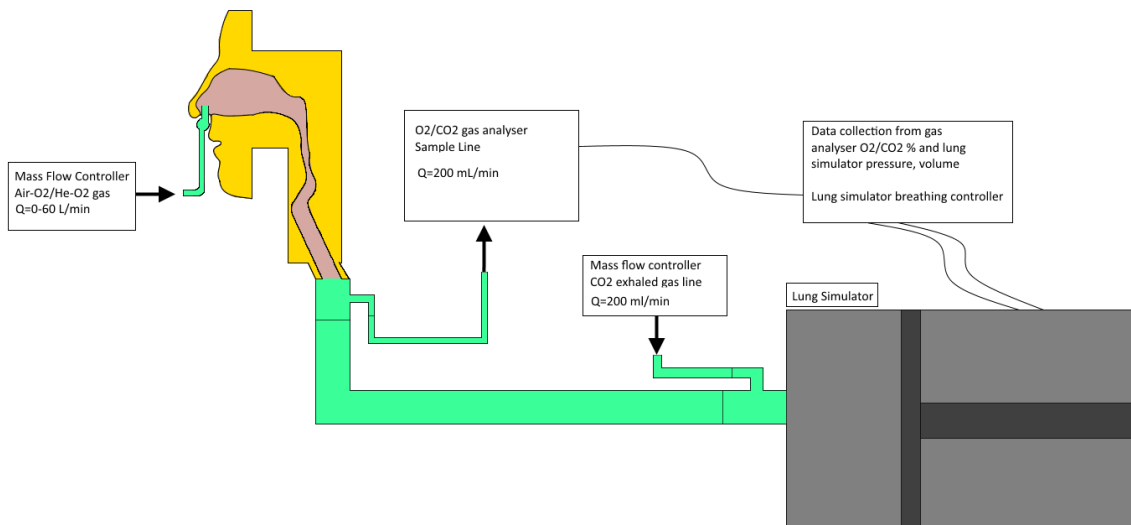


*Figure 3-1: Diagram of experimental setup, HFNC therapy on an upper airway replica served by a breathing lung simulator.*

The experimental apparatus is illustrated in Figure 3-1. In order to simulate adult breathing during administration of high flow therapy, anatomically accurate 3-dimensional replicas of closed-mouth adult airways, extending from nares to trachea, were connected to a lung simulator (ALS 5000; Ingmar Medical Inc., Pittsburg PA USA) at the trachea. These replicas were originally described by Golshahi *et al* (69), and have been used previously for evaluating HFNC

therapy (Moore *et al.* (78)). Upper airways geometries were obtained from magnetic resonance imaging (MRI) scans of adult volunteers breathing tidally in a closed mouth position and were constructed in acrylic plastic. Subject parameters are listed in Table 3-1, as described in Golshahi *et al.* and Moore *et al.* (69, 78). The tubing connecting the trachea to the lung simulator was selected in order to approximate the conducting airway volume between the trachea and terminal bronchioles of a typical adult, with a volume of 182.5 cc, and a length of 46 cm (38). Pressure drop along tubing of this length at peak inspiration is estimated to be 0.9 Pa for the present breathing flowrates and was thus neglected.

*Table 3-1: Rapid prototyped upper airway replica dimensions. Data from Golshahi et al. (69) and Moore et al. (78).*

Subject	Sex	Airway Volume, V (mm <sup>3</sup> )	Nares to Trachea Length, L (mm)	Internal Surface Area, A <sub>s</sub> (mm <sup>2</sup> )	Nares Opening Area, A <sub>n</sub> (mm <sup>2</sup> )	Average Cross Sectional Area, A <sub>c</sub> =V/L (mm <sup>2</sup> )
2	F	44567	241	28718	63.8	185
5	F	35859	210	23532	89.2	171
6	M	50125	269	31345	89.0	186
8	M	47264	223	28936	82.2	212
9	M	45267	239	25086	103.5	189

To simulate high flow therapy, gas was provided through a mass flow controller (MCR-100SLPM-D/5M; ALICAT Inc., AZ USA) at volumetric flow rates of 0, 15, 30 and 60 standard litres per minute (SLPM). Two specialized high flow therapy cannula, Vapotherm Adult and Vapotherm Adult Small (Vapotherm®, Exeter NH USA) and one generic cannula (Adult Nasal Cannula 1104; Teleflex Medical Inc., NC USA) were tested. Cannula dimensions are listed in Table 3-2. Additionally, experiments were conducted for three different gases: air, oxygen and a helium-oxygen mixture (He:O<sub>2</sub>=80:20 by volume). Supplied gases were provided dry, at room

temperature (Praxair Canada Inc, Mississauga, ON Canada). Measurements at 0 SLPM were replicated three times, without repetition between gasses.

*Table 3-2 Cannula Dimensions used in HFNC therapy*

<b>Cannula</b>	<b>Inner Diameter (mm)</b>	<b>Outer Diameter (mm)</b>	<b>Type</b>
<b>Generic Cannula</b>	3.5	4.5	Generic straight
<b>Vapotherm Adult</b>	3.0	4.8	Specialized HFNC
<b>Vapotherm Adult Small</b>	1.9	2.7	Specialized HFNC

The breathing simulator breathing pattern is illustrated in Figure 3-2. The breathing pattern was set to have a tidal volume of  $V_t=0.5$  L, a frequency of  $f=18$  breaths/minute, and inspiratory/expiratory ratio of  $i:e=1:2$ . Parameters were selected to reflect a typical adult tidal breathing pattern, and were similar to those used in previous studies investigating airway pressures delivered during HFNC (25, 78). Volume, flow and pressure parameters were measured by the lung simulator, including tracheal pressure. Breathing parameters, such as PEEP, minimum and maximum pressure, were recorded at the trachea by the lung simulator's proprietary software.

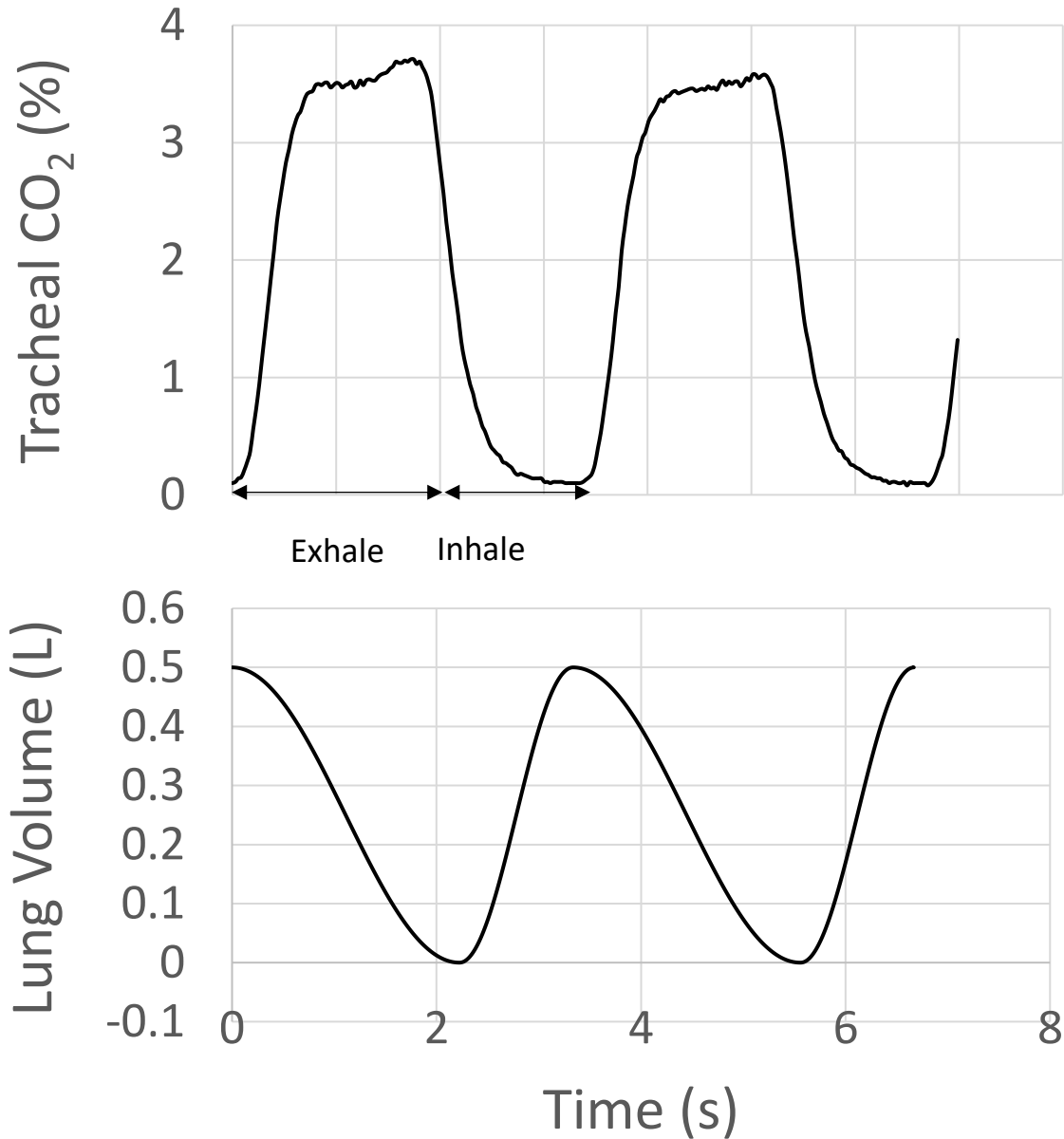


*Figure 3-2: Sample CO<sub>2</sub> concentration (top) and lung volume (bottom) waveforms for the airway replica of subject 2, without HFNC. Alignment of time axes between the two plots was estimated by visual inspection.*

In order to simulate the carbon dioxide (CO<sub>2</sub>) content in exhaled gas, pure CO<sub>2</sub> (Praxair Canada inc., Mississauga ON Canada) was injected at the entrance to the lung simulator. The

flow rate was set at 200 ml/min using a mass flow controller (MCR-20SLPM-D/5M; ALLICAT Inc., AZ USA). This flow was selected to reflect a physiologically relevant rate of CO<sub>2</sub> produced during normal breathing for a minute volume of V<sub>m</sub>=9L, and produced an average per-breath CO<sub>2</sub> content of approximately 2%. A sample tracheal CO<sub>2</sub> trace is shown in Figure 3-2, alongside the volume waveform of the lung simulator. The shape and peak of the waveform are generally in agreement with *in-vivo* capnographs in the literature (37, 82).

CO<sub>2</sub> and O<sub>2</sub> content was measured by a sample line connecting the trachea to a gas analyzer (GA-200; iWorx Systems Inc. NH USA, accurate to 0.01%). The gas analyzer was calibrated for a range of 18.7-99.9% oxygen and 0-10% CO<sub>2</sub>, using the high accuracy setting. Sampling occurred at a flow rate of 200 ml/min to balance the CO<sub>2</sub> flow supplied to the circuit. Sample tests showed negligible influence of sample flow rate on measured CO<sub>2</sub> concentration waveforms. A custom code in the Labview environment (Labview; National Instruments, TX USA) was used to collect oxygen and CO<sub>2</sub> concentrations over time from the gas analyzer at a sample rate of approximately 33 Hz.

In order to reach steady state gas concentrations in the lung simulator, tests were run for a full minute before recording 30 seconds of pressure and gas concentration data. Each combination of test conditions (gas, cannula, replica, flowrate) was repeated three times. Cannula were removed from the replicas and replaced for a given combination of gas type, cannula, and replica after each individual series of measurements spanning HFNC flow rates from 0 to 60 SLPM.

### ***Influence of breathing pattern***

In addition to comparing effects of gas, cannula, airway geometry and flowrate, a comparison of breathing patterns was conducted. The original breathing pattern was modified in two ways that multiplied the minute volume by 1.5. The additional breathing patterns had  $f=27$  breaths/minute and  $V_t=0.5$  L, and  $f=18$  bpm and  $V_t=0.75$  L. These breathing patterns were tested using the Vapotherm Adult cannula and air, for a full range of flowrates. The protocol of recording 30 s of breathing, after steady state conditions were achieved was performed in these tests, with 3 repetitions.

### ***Analytical Methods***

A code was written in the MATLAB® environment (MathWorks Inc., Natick MA USA) to process the CO<sub>2</sub> concentration data. For each experimental repetition, average gas concentration was calculated over each breath and then averaged for the 9 breaths. The inhaled volume of CO<sub>2</sub> was calculated by numerically integrating the CO<sub>2</sub> waveform over the flowrate provided by the lung simulator. The forward rectangle rule was used in this integration. The start of expiration was identified manually in the CO<sub>2</sub> waveform as the local minimum at which point CO<sub>2</sub> content began rising at a rate above 4 %CO<sub>2</sub>/s. The exhalation and inhalation periods are labeled in Figure 3-2.

In order to evaluate the influences of cannula, gas type, flow rate, and replica, a 4-factor ANOVA was performed comparing average CO<sub>2</sub> concentration and PEEP. The Tukey HSD post hoc method was utilized to determine the relative influence of factors. Normality within the replica group was ensured for tracheal clearance data, defined as  $P>0.01$  using the Kolmogorov-Smirnov test. Normality in data was not achieved for CO<sub>2</sub> clearance and PEEP. Equal variance

was violated in clearance time and pressure data, defined as  $P > 0.01$  in the Levene's test, however ANOVA is robust towards mild heteroscedasticity where cells are equal (83). All  $R^2$  values presented are adjusted to account for variable size. Statistical analysis was performed in the SPSS environment (IBM SPSS; IBM Corp., NY USA). Multiple variable linear regression analysis was performed on PEEP to compare the relative influences of flow rate, gas density, gas viscosity and geometric factors, including nares area and path length from the nares to the exit of the replica. Multiple combinations of parameters were compared to determine a simple predictive relationship for PEEP, based on existing fluid mechanical models.

## **Results**

### ***Clearance***

4-way ANOVA shows significant influence of airway geometry, cannula selection, gas selection and HFNC flowrate ( $p < 0.001$ ) as well as all pairwise and triplet interactions ( $p < 0.01$ ). Overall predictive power of the model is  $R^2 = 0.993$ . Post-hoc analysis reveals that although all factors were significant, the influence of cannula was comparatively small, with a mean difference of 0.02%  $\text{CO}_2$  (Generic vs Vapotherm® Adult cannula). This is one-tenth the influence of replica geometry (0.2%  $\text{CO}_2$  comparing subject 6 and 8) and a third that of gas (0.06 %  $\text{CO}_2$  comparing oxygen and He/ $\text{O}_2$ ).

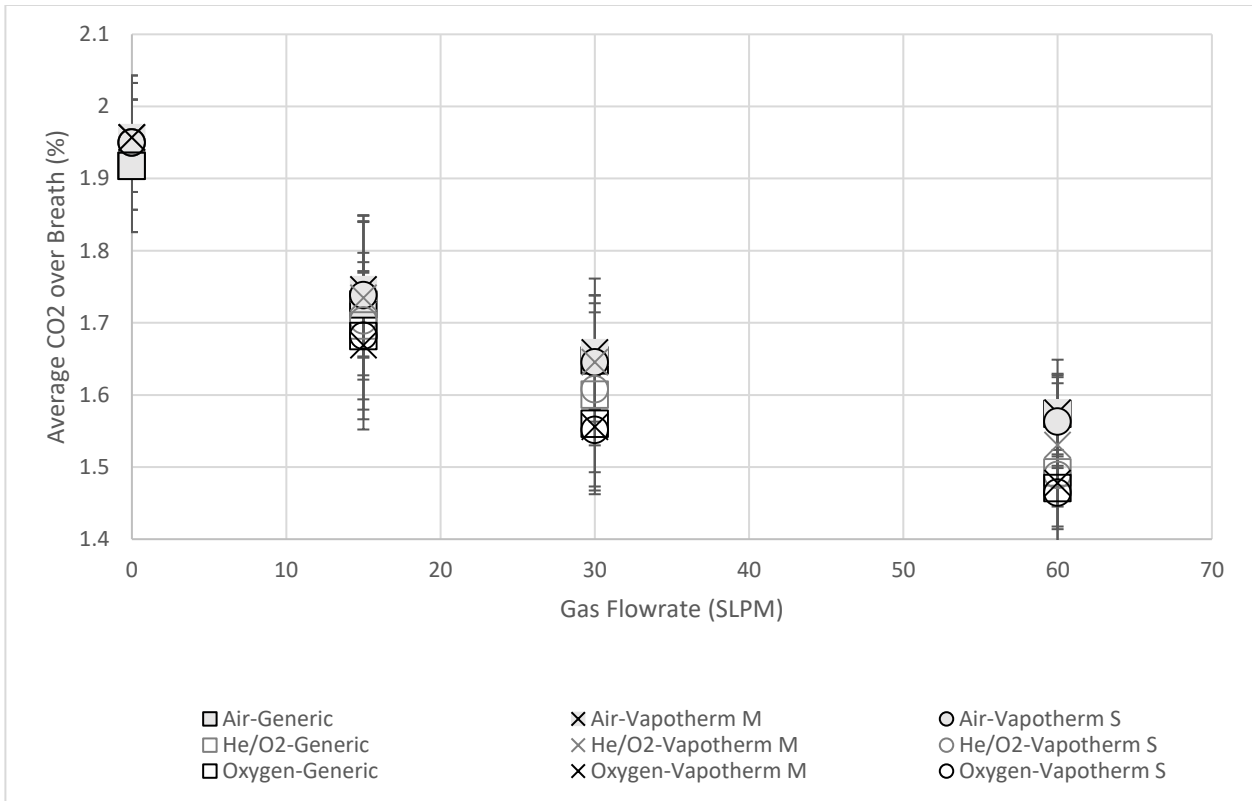
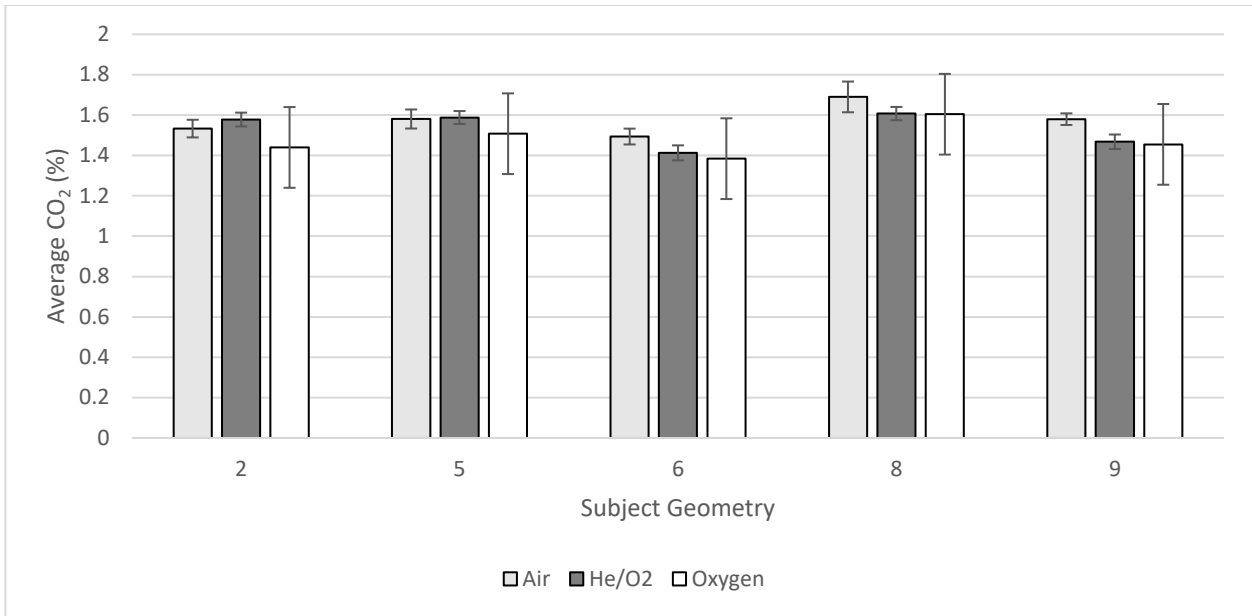


Figure 3-3: Average CO<sub>2</sub> per breath, averaged for all replicas, is presented for different cannula and gas type. Error bars represent standard deviation around the average (n = 5).

The average CO<sub>2</sub> per breath, averaged over all airway geometries, is shown in Figure 3-3. There is a consistent decrease in CO<sub>2</sub> with increasing HFNC flowrate. This decrease appears to taper off at higher flow rates, especially for flows greater than 30 L/min. There is no consistent difference between the three cannula.



*Figure 3-4: Average CO<sub>2</sub> concentration over the breath is compared for individual airway replicas for air, heliox, and oxygen. Values compared were obtained using the Vapotherm Adult Cannula, at 60 LPM flow. Geometry numbers correspond with those listed in Table 3-1. Error bars represent one standard deviation (n=3).*

Figure 3-3 also indicates small but consistent differences between gases when comparing the breath-averaged CO<sub>2</sub> concentration averaged across the five airway replicas, with oxygen producing the lowest average CO<sub>2</sub>, and air producing the greatest. However, Figure 3-4 shows that the influence of gas type was inconsistent between individual airway replicas. Figure 3-4 displays data for the Vapotherm adult cannula and 60 SLPM HFNC flowrate; however, the inconsistent influence of gas type between replicas is representative of all other test conditions. While oxygen delivery produced the lowest average CO<sub>2</sub>, the average CO<sub>2</sub> from tests involving air and heliox are inconsistent, with some geometries indicating a higher and some a lower average CO<sub>2</sub> for air.

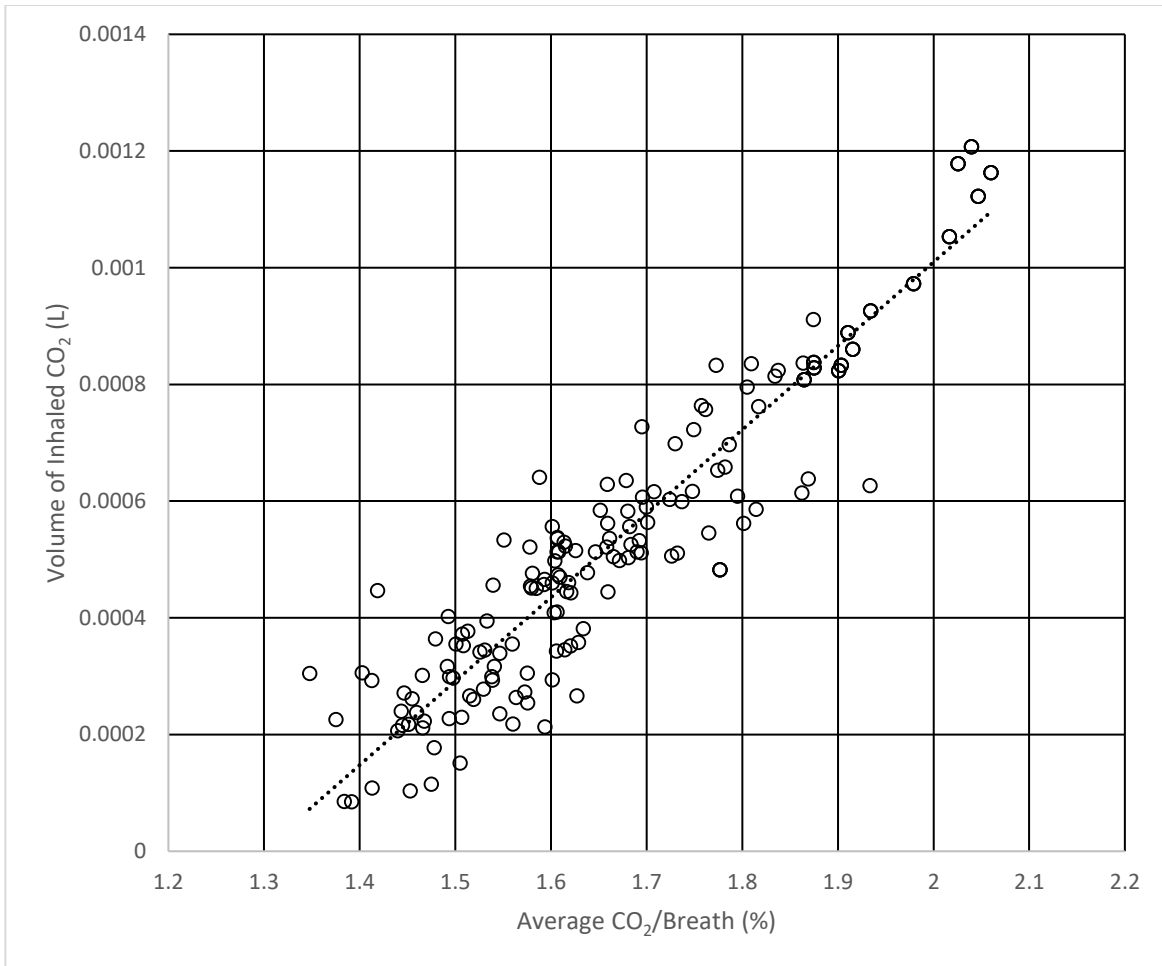


*Figure 3-5: A comparison of estimated inhaled volume of CO<sub>2</sub> and average tracheal CO<sub>2</sub>.*

*Estimated volume of CO<sub>2</sub> was determined numerically, by estimating start of breath and integrating over known breathing pattern. Average CO<sub>2</sub> is a simple time weighted average of CO<sub>2</sub> measured.*

The average inhaled volume of CO<sub>2</sub> was estimated using the known flowrates through the lung simulator. This estimate is compared with average CO<sub>2</sub> per breath in Figure 3-5. Generally, there is a good correlation of  $R^2=0.89$  between the two measures of HFNC clearance. Inhaled volume of CO<sub>2</sub> is of particular interest, as it has direct physiological implications for a patient, both in terms of limiting gas exchange, and by representing O<sub>2</sub> that is not being inhaled. By

correlating inhaled volume of CO<sub>2</sub> to average CO<sub>2</sub>, the easily measured average CO<sub>2</sub> can be compared in the place of the physiologically relevant inhaled volume of CO<sub>2</sub>.

### ***Effect of Minute Volume***

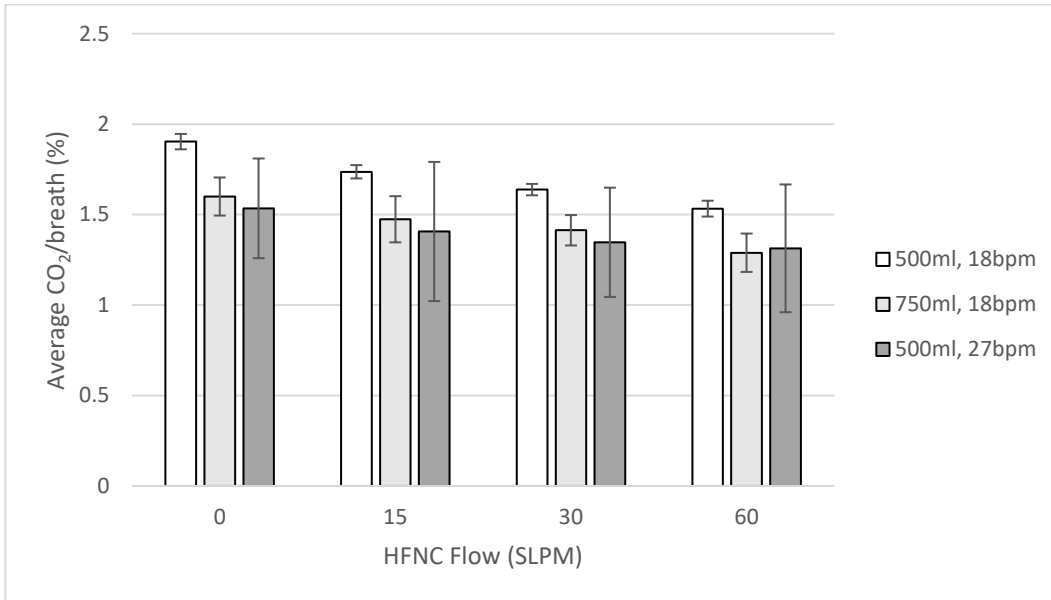


*Figure 3-6: Average CO<sub>2</sub>/breath for the replica geometry of subject 2, using the Vapotherm Adult cannula, with modified breathing patterns. Error bars represent standard deviation of the average of 3 repetitions.*

A comparison of average CO<sub>2</sub> for the V<sub>t</sub>=750 ml and the f=27bpm data can be seen illustrated in Figure 3-6. A reduction in average CO<sub>2</sub> was seen compared to the V<sub>t</sub>=500 ml and f=18 bpm cases. Both the higher frequency and higher tidal volumes result in an approximately equal reduction in average CO<sub>2</sub>. Normalizing average CO<sub>2</sub> to the 0 SLPM HFNC respective test case can be seen in Figure 3-7. In the case of normalized average CO<sub>2</sub> content, there is negligible difference in relative reduction of CO<sub>2</sub>.

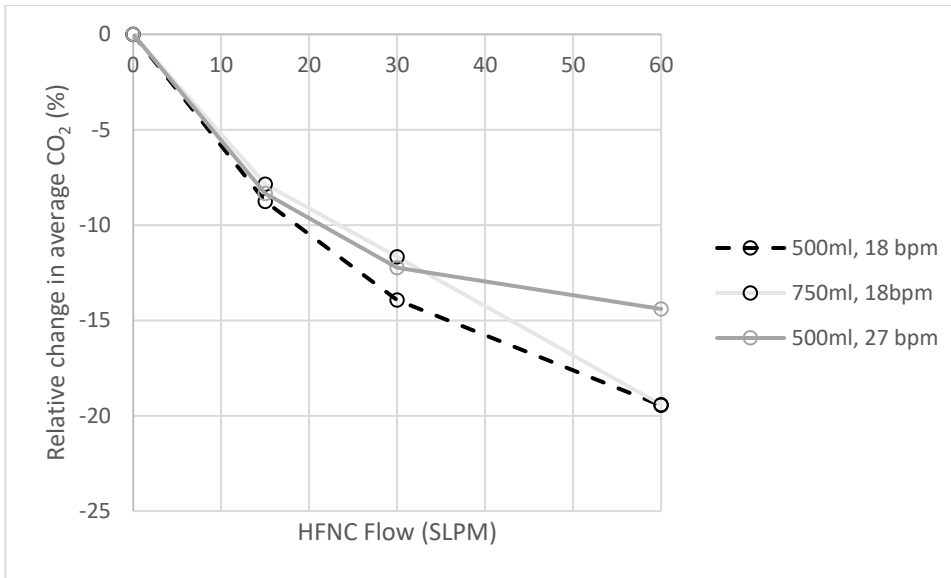


*Figure 3-7: Average relative normalized CO<sub>2</sub>/breath for replica subject 2 geometry, using Vapotherm Adult cannula, with modified breathing patterns. CO<sub>2</sub> normalized to data at 0 L/min HFNC flow. Error bars omitted for clarity, see Figure 3-6 for relative uncertainties in measurement.*

### **Pressure**

The average PEEP of 9 breaths were recorded during HFNC supplied. The average PEEP of all replicas is compared in Figure 3-8. There is a consistent trend of increasing pressure with flow rate. Regression indicates that a quadratic relationship between flow rate and PEEP holds for all cases ( $R^2 > 0.99$ ). Four factor ANOVA of flow rate, gas type, cannula, and replica geometry found each to be significant ( $p < 0.001$ ). Post hoc analysis shows the helium oxygen mixture gives the lowest pressure, and the oxygen gas has the highest pressure ( $p < 0.001$ ), with the tracheal pressure during air HFNC being much closer to that of oxygen than heliox. In all cases, the Vapotherm Adult Small cannula resulted in the highest PEEP, followed by the Vapotherm Adult

Normal, and finally the generic cannula resulted in the lowest pressure ( $p < 0.001$ ). The relative effects of gas and cannula appear to be on the same order of magnitude.

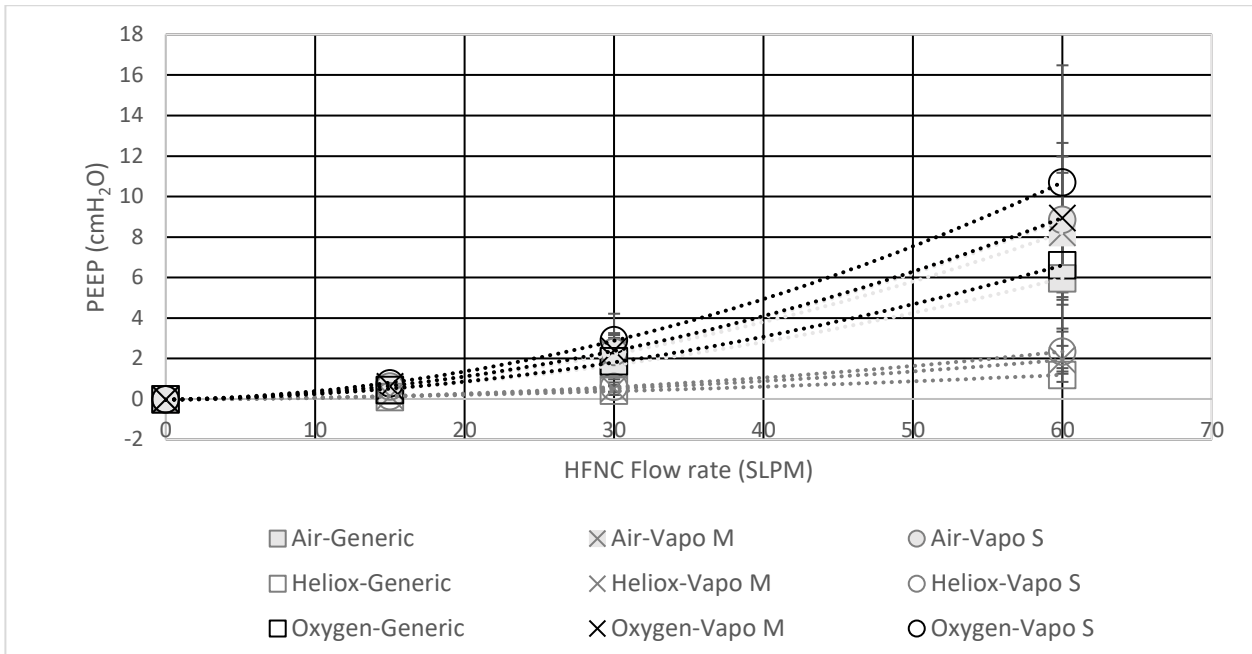


Figure 3-8: Average PEEP for all replica geometries, controlled for cannula and gas selection, compared with HFNC flowrate. Trendlines presented for individual case quadratic best fit. Error bars represent standard deviation around the average ( $n = 5$ ).

The influence of airway geometry is evident in Figure 3-9. The quadratic trend of increasing pressure with respect to HFNC flow rate holds for all five geometries. This trend was suggested in previously published literature (29, 30, 78). The influence of replica geometry is of the same order of magnitude as gas and cannula, with PEEP more than doubling between the lowest pressure replica (subject 9) and the highest (subject 2).

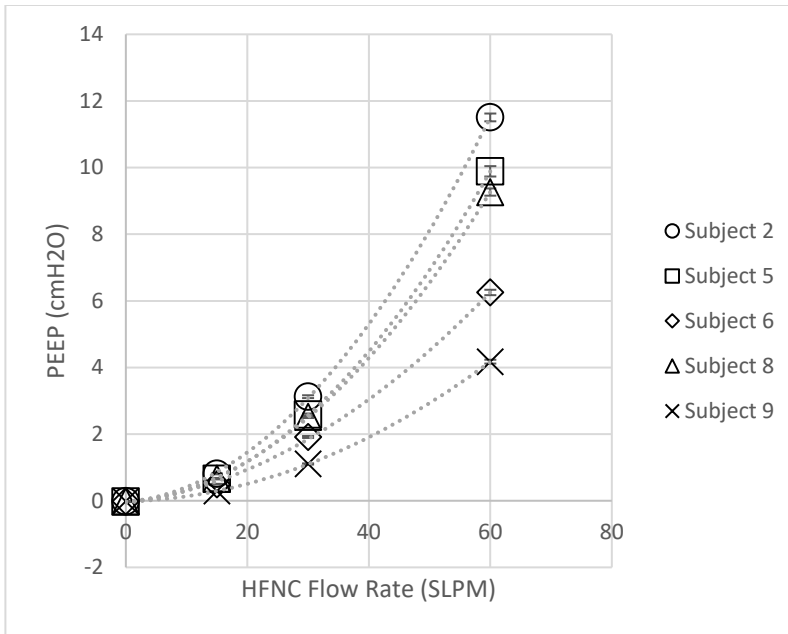


Figure 3-9: Comparison of PEEP with respect to flowrate for each airway geometry. Cases compared are breathing air, with Vapotherm® adult cannula selected. Trendlines presented for individual case quadratic best fit. Error bars represent 1 standard deviation, N=3.

## Discussion

### Factors Influencing Gas Clearance

The ANOVA results demonstrate that the dominant factor in reduction of inhaled CO<sub>2</sub> is the flow rate. The significant decrease in CO<sub>2</sub> with increasing flowrate has been previously documented (30, 84). Additionally, Figure 3-3 gives evidence that the clearance effect asymptotically approaches a local floor value, in agreement with Nielsen *et al.* (30). Figure 3-3 shows this decrease in average CO<sub>2</sub> strongly corresponds with inhaled volume of CO<sub>2</sub>. Clinically, this indicates that cannula flow rates approach 30-60 LPM, there would be diminishing returns associated with further increasing flow rate, so that other considerations such as patient comfort and distending pressure, should take precedence.

Although airway geometry has a definitive influence on gas clearance, the reason for this is not entirely evident. Although the difference in average CO<sub>2</sub> at 60 LPM between geometries has a range of 0.2% with highest and lowest CO<sub>2</sub> (subject 6 and 8), Figure 3-5 shows that this corresponds to a nearly 50% change in inhaled CO<sub>2</sub> volume. No correlation was found between the airway volume, nares to trachea path length, surface area, or nares area with the average CO<sub>2</sub>. This indicates that the influence of airway geometry is more complicated than could be captured using these parameters. One possibility is that the HFNC jet penetration depth is a dominant factor in clearance, with the penetration in turn being affected by airway shape in the form of the size of any pinch point. Although cannula influence was shown to have a weak correlation with airway clearance in Moore *et al.*, the inclusion of breathing in the experiment has further reduced the influence of cannula size (78). Computational simulations of HFNC performed by Van Hove *et al.* show a correlation between volume of inhaled CO<sub>2</sub> and jet penetration (37). Volume of inhaled CO<sub>2</sub> is in turn shown to strongly correlate with average CO<sub>2</sub> per breath in Figure 3-5. The velocity distributions shown by Van Hove *et al.* indicate that the distribution of velocity is heavily influenced by geometry, with the HFNC jet interacting strongly with the nasal concha. These same velocity distributions also show jet penetration changing considerably over the breathing cycle, which may explain the reduced influence of cannula size.

Similarly, ANOVA indicates that although HFNC gas type has a significant effect on clearance, the effect is not consistent. While oxygen has the lowest average CO<sub>2</sub> for all the geometries Figure 3-4 shows that the difference in measured average CO<sub>2</sub> between air and heliox is replica-dependent. The ANOVA results show a strong interaction between gas and airway geometry ( $p < 0.001$ ), reflecting the inconsistent results of gas and airway on CO<sub>2</sub> clearance. The lack of a

meaningful influence of heliox versus air on CO<sub>2</sub> clearance in the present study is consistent with the findings reported by Selium and Sultan, where infants undergoing HFNC with He/O<sub>2</sub> instead of air/O<sub>2</sub> improved PaO<sub>2</sub>, but did not improve PaCO<sub>2</sub> in the blood (81).

The inconsistent interaction of HFNC gas and airway geometry is of interest and highlights the importance of three-dimensional airway structure on convection and diffusion of gases in the nasal airway geometry. Unfortunately, the geometric complexity of these airways requires a large parameter space to capture, making simplistic analysis and explanation elusive. This may explain why there is not a clear correlation of increased mixing with higher Reynolds number.

#### ***Minute Volume Effect on CO<sub>2</sub> Clearance***

Generally, the results shown in Figure 3-6 and Figure 3-7 indicate that minute volume is the determining factor when estimating effect of changing breathing pattern on average CO<sub>2</sub> concentration, at least in the controlled experiments presented here, where CO<sub>2</sub> was injected at a constant rate for all the breathing patterns. However, the decrease in CO<sub>2</sub> relative to baseline values for zero HFNC flow rate was similar for each breathing pattern studied, though this does not account for changes in breathing pattern beyond frequency and tidal volume.

#### ***Constructing a Predictive Model for Pressure***

As mentioned above, there is a consistent quadratic relationship between HFNC flow rate and PEEP. This is reflective of similar patterns found previously in literature (29, 30, 78). Furthermore, previous work by Moore *et al.* identified a correlation to predict PEEP based on the squares of the flow velocities through the cannula and out the nares

$$PEEP = C_1 \rho_{air} u_{nares}^2 + C_2 \rho_{air} u_{cannula}^2 + C_3 \quad [3-1]$$

Where  $u_{nares}$  and  $u_{cannula}$  represent the end-expiratory flow velocities exiting the nares and

entering through the cannula respectively and  $\rho_{air}$  is the density of air (78). The  $C_i$  are constants determined through regression analysis.

The first two terms on the right hand side of Equation (3-1) represent the total static and dynamic pressure in the flow as it enters an airway replica through the cannula. The first term models an orifice-type loss through the annular space between the cannula and nares. Static pressure in the cannula is assumed to increase in order to maintain a constant HFNC flow rate in proportion to this orifice-type loss. The second term represents the dynamic pressure in the flow entering the replica through the cannula. As equation (3-1) was based on experiments performed using air alone, only the density of air appears. In the present study, Figure 3-8 indicates there is a clear influence of gas type on PEEP, with the densest gas appearing to deliver the greatest pressure at a given HFNC flow rate. Therefore, to best predict PEEP for the present data set gas density was included as a variable in equation (3-2) below.

$$PEEP = 0.018\rho_g u_{cannula}^2 + 0.726\rho_g u_{nares}^2 + 23.8 \text{ Pa} \quad [3-2]$$

Including gas density considerably improved the prediction of PEEP ( $R^2=0.759$  for equation (3-2), compared with  $R^2=0.514$  for equation (3-1) with best-fit constants). This provides evidence that the correlation originally described by Moore *et al.* can be extended to other gases and cannula types (78). Furthermore, the magnitude of the third term is small, on the scale of pressures at 15 LPM (23.8Pa=0.243 cmH<sub>2</sub>O, compared with the average pressure at 15 LPM flow using heliox and air of 0.123 cmH<sub>2</sub>O and 0.542 cmH<sub>2</sub>O respectively). This term exists primarily as an empirical correction to the minor losses model proposed here, which accounts for other possible losses and may correct where the model does not fit perfectly.

## Conclusion

In the present study, the average upper airway CO<sub>2</sub> concentration during tidal breathing decreased as the HFNC flow rate increased. The marginal decrease in CO<sub>2</sub> decreased with increasing flowrate above 30 l/min. Compared with HFNC flow rate, cannula size and delivered gas type had only minor influence on upper airway CO<sub>2</sub> concentration.

In contrast, HFNC flow rate, cannula size, and gas type, all had notable influence on tracheal pressure. Tracheal PEEP increased with HFNC flow rate in an approximately quadratic pattern over the range of flow rates studied here (15 to 60 l/min). Additionally, the less dense gas, heliox, considerably reduced PEEP. Confirming findings in previous studies, smaller cannula also resulted in greater PEEP (78). A predictive correlation for PEEP was proposed, based on the gas density and the squares of gas velocities entering the nares through the cannula and exiting the nares around the cannula. The inclusion of gas density in this correlation improved the correlation compared to predictions which do not include a gas density term. Compared with HFNC administration of air or oxygen, HFNC administration of heliox is expected to result in similar CO<sub>2</sub> clearance from the upper airway, but markedly lower positive airway pressure.

## Chapter 4 Conclusions and Recommendations

### Summary

This thesis is a collection of published and submitted works, aimed to characterize the pressure and washout effects of high flow nasal cannula (HFNC) therapy. Positive airway pressure and washout of exhaled air are two of the proposed primary mechanisms by Dysart *et al.* by which HFNC therapy treats respiratory distress (1). These characterizations of pressure and washout effects of HFNC may be used to aid in the creation of device specific guidelines for clinical environments. Furthermore, the ability to predict the relative changes in pressure and washout delivered by HFNC will allow for improved design of delivery devices. The relationships here account for intersubject variability in airway geometry, as well as the specifics of HFNC delivery.

Airway washout of exhaled air was modeled in two phases. The first considered a non-breathing model where the time to purge an upper airway model of air, while delivering HFNC, was considered. Five airway geometries were compared for intersubject differences, as well as three commercial cannulas, and flowrates ranging from 30-90 L/min. Using 3-way ANOVA, it was determined that cannula design, flowrate and airway geometry were relevant factors in determining washout time of the non-breathing upper airways. Furthermore, this washout correlated strongly with higher flowrates and more weakly with decreasing cannula size.

The second phase of investigating upper airway washout involved measuring washout during tidal breathing, through the measurement of CO<sub>2</sub> content. The same upper airway geometries were compared, and in addition to three cannula and flowrates ranging from 0-60 L/min, air, oxygen and heliox (He/O<sub>2</sub>:80/20) were also compared. Post-hoc analysis revealed that gas

flowrate was the dominant factor in determining washout, with comparatively weaker influences from gas and airway geometry. Comparatively less change in average CO<sub>2</sub> was observed when comparing flowrates above 30 L/min. Changes in minute volume had no significant effect on CO<sub>2</sub> washout.

The positive end expiratory pressure (PEEP) was also measured in the same five upper airway geometries, while breathing was at a set rate. A predictive correlation based on minor losses was constructed to predict PEEP when breathing air. The minor losses were based on flow velocities in the cannula and nares. In the second phase of research, this predictive correlation was extended to account for gas densities.

### **Future Work**

In this study, experiments were performed to measure the positive airway pressure and gas washout in adult airway replicas. Further analysis of the existing gas clearance data presented in Chapter 3 will allow for possible prediction of changes in inhaled CO<sub>2</sub> volume. Additionally, the analysis of pressure presented in Chapter 3 leaves room for improvement, such as by better accounting for laminar minor losses.

This study focused exclusively on adult upper airway replicas, and thus conclusions cannot be extended to other age categories, such as infants. It is possible that the conclusions relating to both upper airway washout and positive pressure during HFNC delivery cannot be extended to infant airways, due in part to their different size, shape and breathing pattern. These experiments could be extended to use upper airway replicas of infants and children under administration of HFNC therapy. The use of helium-oxygen mixtures is of particular interest to pediatric patients, where reducing airway resistance is more important in the treatment of

respiratory distress. Of the experiments involving breathing, only constant volume breathing was considered. This is not physiologically accurate, especially as breathing is adaptive to environment.

This study uses *in vitro* replicas of upper airways. *In vivo* experiments are recommended to specifically validate the existing predictions more thoroughly, especially with respect to controlling breathing in patients. Historically, although *in vivo* experiments have been conducted to measure washout and positive airway pressure, direct and controlled experiments are costly and complicated. Special attention should be given to HFNC device specific effects.

## Works Cited

1. Dysart K, Miller TL, Wolfson MR, Shaffer TH. Research in high flow therapy: Mechanisms of action. *Respiratory Medicine*. 2009 October;103(10):1400-5.
2. Zhang J, Lin L, Pan K, Zhou J, Huang X. High-flow nasal cannula therapy for adult patients. *Journal of International Medical Research*. 2016;44(6):1200-11.
3. Nishimura M. High-flow nasal cannula oxygen therapy in adults. *Journal of intensive care*. 2015;3(1):15.
4. Helviz Y, Einav S. A Systematic Review of the High-flow Nasal Cannula for Adult Patients. *Critical care (London, England)*. 2018 Mar 20;;22(1):71.
5. Fricke K, Tatkov S, Domanski U, Franke K, Nilius G, Schneider H. Nasal high flow reduces hypercapnia by clearance of anatomical dead space in a COPD patient. *Respiratory Medicine Case Reports*. 2016;19:115-7.
6. Nilius G, Franke K, Domanski U, Rühle K, Kirkness JP, Schneider H. Effects of nasal insufflation on arterial gas exchange and breathing pattern in patients with chronic obstructive pulmonary disease and hypercapnic respiratory failure. *Advances in experimental medicine and biology*. 2013;755:27.
7. Sztrymf B, Messika J, Mayot T, Lenglet H, Dreyfuss D, Ricard J. Impact of high-flow nasal cannula oxygen therapy on intensive care unit patients with acute respiratory failure: A prospective observational study. *Journal of Critical Care*. 2012 June;27(3):324.e13.
8. Messika J, Ben Ahmed K, Gaudry S, Miguel-Montanes R, Rafat C, Sztrymf B, et al. Use of High-Flow Nasal Cannula Oxygen Therapy in Subjects With ARDS: A 1-Year Observational Study. *Respiratory care*. 2015 Feb;60(2):162-9.
9. Simon M, Braune S, Frings D, Wiontzek A, Klose H, Kluge S. High-flow nasal cannula oxygen versus non-invasive ventilation in patients with acute hypoxaemic respiratory failure undergoing flexible bronchoscopy - a prospective randomised trial. *Critical Care*. 2014 Dec 1;;18(6).
10. Ni Y, Luo J, Yu H, Liu D, Ni Z, Cheng J, et al. Can High-flow Nasal Cannula Reduce the Rate of Endotracheal Intubation in Adult Patients With Acute Respiratory Failure Compared With Conventional Oxygen Therapy and Noninvasive Positive Pressure Ventilation?: A Systematic Review and Meta-analysis. *Chest*. 2017 Apr;151(4):764.
11. Ou X, Hua Y, Liu J, Gong C, Zhao W. Effect of high-flow nasal cannula oxygen therapy in adults with acute hypoxemic respiratory failure: a meta-analysis of randomized controlled

trials. CMAJ : Canadian Medical Association journal = journal de l'Association medicale canadienne. 2017 Feb 21,;189(7):E267.

12. Monro-Somerville T, Sim M, Ruddy J, Vilas M, Gillies M. The Effect of High-Flow Nasal Cannula Oxygen Therapy on Mortality and Intubation Rate in Acute Respiratory Failure: A Systematic Review and Meta-Analysis. *Critical Care Medicine*. 2016 Sep 8,;45(4):e456.

13. Frat J, Thille AW, Mercat A, Girault C, Ragot S, Perbet S, et al. High-Flow Oxygen through Nasal Cannula in Acute Hypoxemic Respiratory Failure. *New England Journal of Medicine*. 2015 June 4,;372(23):2185-96.

14. Rittayamai N, Tscheikuna J, Rujiwit P. High-flow nasal cannula versus conventional oxygen therapy after endotracheal extubation: a randomized crossover physiologic study. *Respiratory care*. 2014 Apr;59(4):485-90.

15. Zhao H, Wang H, Sun F, Lyu S, An Y. High-flow nasal cannula oxygen therapy is superior to conventional oxygen therapy but not to noninvasive mechanical ventilation on intubation rate: a systematic review and meta-analysis. *Critical Care*. 2017 Jul 1,;21.

16. Miguel-Montanes R, Hajage D, Messika J, Bertrand F, Gaudry S, Rafat C, et al. Use of High-Flow Nasal Cannula Oxygen Therapy to Prevent Desaturation During Tracheal Intubation of Intensive Care Patients With Mild-to-Moderate Hypoxemia. *Critical Care Medicine*. 2015 Mar;43(3):574-83.

17. Joakim Engström, Göran Hedenstierna, Anders Larsson. Pharyngeal oxygen administration increases the time to serious desaturation at intubation in acute lung injury: an experimental study. *Critical Care [NLM - MEDLINE]*. 2010 Jan 1,;14(3):R93.

18. McGinley BM, Patil SP, Kirkness JP, Smith PL, Schwartz AR, Schneider H. A Nasal Cannula Can Be Used to Treat Obstructive Sleep Apnea. *American Journal of Respiratory and Critical Care Medicine*. 2007 Jul 15,;176(2):194-200.

19. Haba-Rubio J, Andries D, Rey V, Michel P, Tafti M, Heinzer R. Effect of transnasal insufflation on sleep disordered breathing in acute stroke: a preliminary study. *Sleep Breath*. 2012 Sep;16(3):759-64.

20. Rea H, McAuley S, Jayaram L, Garrett J, Hockey H, Storey L, et al. The clinical utility of long-term humidification therapy in chronic airway disease. *Respiratory Medicine*. 2010;104(4):525-33.

21. Kushida CA, Chediak A, Berry RB, Brown LK, Gozal D, Iber C, et al. Clinical Guidelines for the Manual Titration of Positive Airway Pressure in Patients with Obstructive Sleep Apnea. *Journal of Clinical Sleep Medicine*. 2008;4(2):157-71.

22. Parke RL, McGuinness SP. Pressures delivered by nasal high flow oxygen during all phases of the respiratory cycle. *Respiratory care*. 2013 Oct;58(10):1621-4.
23. Parke R, McGuinness S, Eccleston M. Nasal high-flow therapy delivers low level positive airway pressure. *Br J Anaesth*. 2009 Dec;103(6):886-90.
24. Frizzola M, Miller TL, Rodriguez ME, Zhu Y, Rojas J, Hesek A, et al. High-flow nasal cannula: Impact on oxygenation and ventilation in an acute lung injury model. *Pediatr Pulmonol*. 2011 January 1;46(1):67-74.
25. Chanques G, Riboulet F, Molinari N, Carr J, Jung B, Prades A, et al. Comparison of three high flow oxygen therapy delivery devices: a clinical physiological cross-over study. *Minerva Anestesiologica*. 2013 December;79:1344-55.
26. Parke RL, Eccleston ML, McGuinness SP. The effects of flow on airway pressure during nasal high-flow oxygen therapy. *Respiratory care*. 2011 Aug;56(8):1151-5.
27. Groves N, Tobin A. High flow nasal oxygen generates positive airway pressure in adult volunteers. *Australian Critical Care*. 2007;20(4):126-31.
28. Kubicka ZJ, Limauro J, Darnall RA. Heated, Humidified High-Flow Nasal Cannula Therapy: Yet Another Way to Deliver Continuous Positive Airway Pressure? *Pediatrics*. 2008 Jan 1;121(1):82.
29. Luo J, Lu M, Zhao Z, Jiang W, Xu B, Weng L, et al. Positive End-Expiratory Pressure Effect of 3 High-Flow Nasal Cannula Devices. *Respiratory Care*. 2017 Jul;62(7):888-95.
30. Nielsen KR, Ellington LE, Gray AJ, Stanberry LI, Smith LS, DiBlasi RM. Effect of High-Flow Nasal Cannula on Expiratory Pressure and Ventilation in Infant, Pediatric, and Adult Models. *Respiratory Care*. 2018 Feb;63(2):147-57.
31. Parke RL. Effect of Very-High-Flow Nasal Therapy on Airway Pressure and End-Expiratory Lung Impedance in Healthy Volunteers. *Respiratory Care*. 2015 October;60(10):1397-403.
32. Kumar H, Spence CJT, Tawhai MH. Modeling the pharyngeal pressure during adult nasal high flow therapy. *Respiratory physiology & neurobiology*. 2015 Dec;219:51-7.
33. Miller TL, Saberi B, Saberi S. Computational Fluid Dynamics Modeling of Extrathoracic Airway Flush: Evaluation of High Flow Nasal Cannula Design Elements. *Journal of Pulmonary & Respiratory Medicine*. 2016;6(5).
34. Roca O, Hernández G, Díaz-Lobato S, Carratalá JM, Gutiérrez RM, Masclans JR. Current evidence for the effectiveness of heated and humidified high flow nasal cannula supportive therapy in adult patients with respiratory failure. *Critical care (London, England)*. 2016;20(1):109.

35. Corley A, Caruana LR, Barnett AG, Tronstad O, Fraser JF. Oxygen delivery through high-flow nasal cannulae increase end-expiratory lung volume and reduce respiratory rate in post-cardiac surgical patients. *Br J Anaesth*. 2011 Dec;107(6):998-1004.
36. Sivieri EM, Foglia EE, Abbasi S. Carbon dioxide washout during high flow nasal cannula versus nasal CPAP support: An in vitro study. *Pediatric Pulmonology*. 2017 Jun;52(6):792-8.
37. Van Hove S, Storey J, Adams C, Dey K, Geoghegan P, Kabaliuk N, et al. An Experimental and Numerical Investigation of CO<sub>2</sub> Distribution in the Upper Airways During Nasal High Flow Therapy. *Ann Biomed Eng*. 2016 Oct;44(10):3007-19.
38. Finlay WH. The mechanics of inhaled pharmaceutical aerosols : an introduction. San Diego: Academic Press; 2001.
39. Martini FH, Nath JL, Bartholomew EF. Fundamentals of Anatomy & Physiology. 9th ed. San Francisco, CA: Benjamin Cummings; 2012.
40. Hemph AB, Jakobsson JG. Helium–oxygen mixture for treatment in upper airway obstruction; a mini-review. *Journal of Acute Medicine*. 2016;6(4):77-81.
41. Hashemian SM, Fallahian F. The use of heliox in critical care. *Int J Crit Illn Inj Sci*. 2014;4(2):138-42.
42. Jolliet P, Ouanes-Besbes L, Abroug F, Ben Khelil J, Besbes M, Garnero A, et al. A Multicenter Randomized Trial Assessing the Efficacy of Helium/Oxygen in Severe Exacerbations of Chronic Obstructive Pulmonary Disease. *American journal of respiratory and critical care medicine*. 2017 Apr 1;195(7):871-80.
43. Abroug F, Ouanes-Besbes L, Hammouda Z, Benabidallah S, Dachraoui F, Ouanes I, et al. Noninvasive ventilation with helium-oxygen mixture in hypercapnic COPD exacerbation: aggregate meta-analysis of randomized controlled trials. *Annals of intensive care*. 2017 Dec;7(1):59.
44. Leatherman JW, Romero RS, Shapiro RS. Lack of Benefit of Heliox During Mechanical Ventilation of Subjects With Severe Air-Flow Obstruction. *Respiratory care*. 2018 Apr;63(4):375-9.
45. Martin AR, Katz IM, Terzibachi K, Gouinaud L, Caillibotte G, Texereau J. Bench and mathematical modeling of the effects of breathing a helium/oxygen mixture on expiratory time constants in the presence of heterogeneous airway obstructions. *Biomedical engineering online*. 2012 May 30;11(1):27.

46. Martin AR, Katz IM, Jenöfi K, Caillibotte G, Brochard L, Texereau J. Bench experiments comparing simulated inspiratory effort when breathing helium-oxygen mixtures to that during positive pressure support with air. *BMC Pulmonary Medicine*. 2012 Jan 1,;12(1):62.
47. Zhao K, Jiang J. What is normal nasal airflow? A computational study of 22 healthy adults. *International Forum of Allergy & Rhinology*. 2014 Jun;4(6):435-46.
48. Ishikawa S, Nakayama T, Watanabe M, Matsuzawa T. Visualization of Flow Resistance in Physiological Nasal Respiration: Analysis of Velocity and Vorticities Using Numerical Simulation. *Archives of Otolaryngology–Head & Neck Surgery*. 2006 Nov 1,;132(11):1203-9.
49. Pedley TJ, Schroter RC, Sdulow MF. Energy Losses and Pressure Drop in Models of Human Airways. *Respiratory Physiology*. 1970;9:371-87.
50. Wells AK, Jones IP, Hamill IS, Bordas R. The prediction of viscous losses and pressure drop in models of the human airways. *International Journal for Numerical Methods in Biomedical Engineering*. 2018 Jan;34(1):n/a.
51. Pitts WM. Reynolds number effects on the mixing behavior of axisymmetric turbulent jets. *Experiments in Fluids*. 1991 May;11-11(2-3):135-41.
52. Golshahi L, Noga M, Vehring R, Finlay W. An In vitro Study on the Deposition of Micrometer-Sized Particles in the Extrathoracic Airways of Adults During Tidal Oral Breathing. *Ann Biomed Eng*. 2013 May;41(5):979-89.
53. Golshahi L, Noga ML, Finlay WH. Deposition of inhaled micrometer-sized particles in oropharyngeal airway replicas of children at constant flow rates. *Journal of Aerosol Science*. 2012 July;49:21-31.
54. Golshahi L, Finlay WH, Olfert JS, Thompson RB, Noga ML. Deposition of Inhaled Ultrafine Aerosols in Replicas of Nasal Airways of Infants. *Aerosol Science and Technology*. 2010 August 9,;44(9):741-52.
55. Storey-Bishoff J, Noga M, Finlay WH. Deposition of micrometer-sized aerosol particles in infant nasal airway replicas. *Journal of Aerosol Science*. 2008;39(12):1055-65.
56. Yang MY, Ruzycki C, Verschuer J, Katsifis A, Eberl S, Wong K, et al. Examining the ability of empirical correlations to predict subject specific in vivo extrathoracic aerosol deposition during tidal breathing. *Aerosol Science and Technology*. 2017 Mar 4,;51(3):363-14.
57. Nagata K, Morimoto T, Fujimoto D, Otoshi T, Nakagawa A, Otsuka K, et al. Efficacy of High-Flow Nasal Cannula Therapy in Acute Hypoxemic Respiratory Failure: Decreased Use of Mechanical Ventilation. *Respiratory Care*. 2015 October;60(10):1390-6.

58. Matthay MA, Ware LB, Zimmerman GA. The acute respiratory distress syndrome. *J Clin Invest.* 2012 -8-1;122(8):2731-40.
59. Vargas F, Saint-Leger M, Boyer A, Hilbert G. Physiologic Effects of High-Flow Nasal Cannula Oxygen in Critical Care Subjects. *Respiratory Care.* 2015 October;60(10):1369-76.
60. Cuquemelle E, Papon J, Louis B, Danin P, Brochard L. Heated and Humidified High-Flow Oxygen Therapy Reduces Discomfort During Hypoxemic Respiratory Failure. *Respiratory Care.* 2012 October;57(10):1571-7.
61. Maggiore SM, Idone FA, Vaschetto R, Festa R, Cataldo A, Antonicelli F, et al. Nasal High-Flow versus Venturi Mask Oxygen Therapy after Extubation. Effects on Oxygenation, Comfort, and Clinical Outcome. *Am J Respir Crit Care Med.* 2014 July 8;190(3):282-8.
62. Roca O, Riera J, Torres F, Masclans JR. High-flow oxygen therapy in acute respiratory failure. *Respiratory Care.* 2010 April;55(4):408-13.
63. Spoletini G, Alotaibi M, Blasi F, Hill NS. Heated humidified high-flow nasal oxygen in adults: Mechanisms of action and clinical implications. *Chest.* 2015 July 1;148(1):253-61.
64. Roberts CD, Oeckler RA. A Skeptical Perspective on High-Flow Nasal Cannula in the Treatment of Acute Hypoxemic Respiratory Failure. *Respiratory Care.* 2015 October;60(10):1522-5.
65. Möller W, Celik G, Feng S, Bartenstein P, Meyer G, Oliver E, et al. Nasal high flow clears anatomical dead space in upper airway models. *Journal of applied physiology (Bethesda, Md. : 1985).* 2015 Jun 15;118(12):1525.
66. Golshahi L, Walenga RL, Longest PW, Hindle M. Development of a Transient Flow Aerosol Mixer-Heater System for Lung Delivery of Nasally Administered Aerosols Using a Nasal Cannula. *Aerosol Science and Technology.* 2014 Oct 3;48(10):1009-21.
67. Golshahi L, Longest PW, Azimi M, Syed A, Hindle M. Intermittent aerosol delivery to the lungs during high-flow nasal cannula therapy. *Respiratory care.* 2014 Oct;59(10):1476.
68. Gardner M, Longest PW, Golshahi L. Understanding High-Flow Nasal Cannula Noninvasively With an In Vitro Breathing Infant Lung Model. *Critical Care Medicine.* 2016 Dec;44(12 Suppl 1):337.
69. Golshahi L, Noga ML, Thompson RB, Finlay WH. In vitro deposition measurement of inhaled micrometer-sized particles in extrathoracic airways of children and adolescents during nose breathing. *Journal of Aerosol Science.* 2011 July;42(7):474-88.

70. Arora B, Mahajan P, Zidan M, Sethuraman U. Nasopharyngeal Airway Pressures in Bronchiolitis Patients Treated With High-Flow Nasal Cannula Oxygen Therapy. *Pediatric Emergency Care*. 2012 Nov;28(11):1179-84.
71. Scherer PW, Haselton FR. Convective exchange in oscillatory flow through bronchial-tree models. *Journal of Applied Physiology*. 1982 Oct 1;53(4):1023-33.
72. Nishimura M. High-flow nasal cannula oxygen therapy in adults. *Journal of intensive care*. 2015;3(1):15.
73. Miller TL, Saberi B, Saberi S. Computational Fluid Dynamics Modeling of Extrathoracic Airway Flush: Evaluation of High Flow Nasal Cannula Design Elements. *Journal of Pulmonary & Respiratory Medicine*. 2016;6(5).
74. Tennekes H, Lumley JL. *A first course in turbulence*. Cambridge, MA: MIT Press; 1972.
75. Di mussi R, Spadaro S, Stripoli T, Volta CA, Trerotoli P, Pierucci P, et al. High-flow nasal cannula oxygen therapy decreases postextubation neuroventilatory drive and work of breathing in patients with chronic obstructive pulmonary disease. *Critical Care*. 2018 Jan 1;22(1):1-11.
76. Hernández G, Vaquero C, Colinas L, Cuenca R, González P, Canabal A, et al. Effect of Postextubation High-Flow Nasal Cannula vs Noninvasive Ventilation on Reintubation and Postextubation Respiratory Failure in High-Risk Patients: A Randomized Clinical Trial. *JAMA*. 2016 Oct 18;316(15):1565-74.
77. Maggiore SM, Idone FA, Vaschetto R, Festa R, Cataldo A, Antonicelli F, et al. Nasal high-flow versus Venturi mask oxygen therapy after extubation. Effects on oxygenation, comfort, and clinical outcome. *American journal of respiratory and critical care medicine*. 2014 Aug 1;190(3):282-8.
78. Moore CP, Katz IM, Caillibotte G, Finlay WH, Martin AR. Correlation of high flow nasal cannula outlet area with gas clearance and pressure in adult upper airway replicas. *Clinical Biomechanics*. 2017 Nov 11,.
79. Jassar RK, Vellanki H, Zhu Y, Heseck A, Wang J, Rodriguez E, et al. High flow nasal cannula (HFNC) with Heliox decreases diaphragmatic injury in a newborn porcine lung injury model. *Pediatric Pulmonology*. 2014 Dec;49(12):1214-22.
80. Kim IK, Phrampus E, Sikes K, Pendleton J, Saville A, Corcoran T, et al. Helium-Oxygen Therapy for Infants With Bronchiolitis: A Randomized Controlled Trial. *Archives of Pediatrics & Adolescent Medicine*. 2011 Dec 5;165(12):1115-22.

81. Seliem W, Sultan AM. Heliox delivered by high flow nasal cannula improves oxygenation in infants with respiratory syncytial virus acute bronchiolitis. *Jornal de Pediatria*. 2018 Jan;94(1):56-61.
82. Gravenstein JS, Jaffe MB, Gravenstein N, Paulus DA. *Capnography*. 2nd ed. Cambridge MA: Cambridge University Press; 2011.
83. Malwane A, Weerahandi S. Two-Way Anova With Unequal Cell Frequencies and Unequal Variances. *Statistica Sinica*. 1997 July 1;7(3):631-46.
84. Bräunlich J, Köhler M, Wirtz H. Nasal highflow improves ventilation in patients with COPD. *International journal of chronic obstructive pulmonary disease*. 2016;11:1077-85.

## Appendix A Raw Data for Chapter 2

Table A-1: Clearance time data from non-breathing tests presented in Chapter 2. Each test was repeated 5 times.

Subject	Cannula	O2 Flow (SLPM)	Tracheal Clearance Time 25-50% (s)	Tracheal Clearance Time 25-75% (s)	Tracheal Clearance Time 25-95% (s)	Laryngeal Clearance Time 25-50% (s)	Laryngeal Clearance Time 25-75% (s)	Laryngeal Clearance Time 25-95% (s)
2	Large	30	2.237	6.63	16.82	1.12	2.985	12.868
2	Large	30	2.841	6.487	14.638	1.38	3.196	10.61
2	Large	30	6.974	10.246	17.352	1.667	3.85	10.574
2	Large	30	3.643	7.347	15.757	1.064	2.413	9.771
2	Large	30	4.572	8.705	20.102	1.293	2.942	8.949
2	Large	60	3.215	6.402	13.561	1.608	3.736	10.516
2	Large	60	2.87	6.629	15.182	0.919	2.127	7.212
2	Large	60	2.5	6.615	17.502	1.149	2.383	7.647
2	Large	60	3.342	6.527	13.544	1.874	3.912	12.072
2	Large	60	5.951	9.654	17.836	1.091	2.789	10.778
2	Large	90	2.325	6.545	17.679	0.776	1.782	4.484
2	Large	90	2.927	6.575	14.809	1.236	2.415	5.193
2	Large	90	3.511	6.696	13.728	0.66	1.657	5.997
2	Large	90	2.842	6.517	14.533	1.236	2.989	6.375
2	Large	90	3.273	6.459	13.577	1.033	2.843	10.109
2	Medium	30	2.669	6.287	14.409	0.689	1.636	8.639
2	Medium	30	1.979	6.112	17.336	0.746	2.122	11.26
2	Medium	30	2.868	6.485	14.56	0.689	1.636	6.315
2	Medium	30	3.244	6.401	13.41	0.804	2.297	11.31
2	Medium	30	2.906	6.495	14.561	0.604	1.493	4.342
2	Medium	60	2.008	5.999	17.25	0.774	2.239	10.476
2	Medium	60	2.881	6.554	14.819	0.66	1.927	11.224
2	Medium	60	3.186	6.256	13.23	0.544	1.463	4.652
2	Medium	60	2.871	6.401	14.388	0.516	1.407	4.94
2	Medium	60	1.922	5.998	17.193	0.661	1.522	5.806
2	Medium	90	2.611	6.086	13.864	0.717	1.721	8.207
2	Medium	90	5.654	8.641	15.14	0.63	1.55	9.854
2	Medium	90	3.16	6.145	12.837	0.633	1.467	10.052
2	Medium	90	3.099	6.058	12.772	0.633	1.495	7.617
2	Medium	90	2.699	6.23	14.265	0.631	1.55	8.554
2	Small	30	2.323	7.318	18.569	0.776	1.869	7.058
2	Small	30	2.586	6.094	14.284	0.948	2.44	11.661
2	Small	30	2.007	5.859	17.077	0.833	1.868	6.855

2	Small	30	2.726	6.314	14.465	0.862	2.153	9.815
2	Small	30	1.867	5.97	17.367	0.804	1.868	6.58
2	Small	60	2.726	6.315	14.61	0.776	2.271	11.89
2	Small	60	1.867	5.913	17.138	0.746	1.781	6.152
2	Small	60	2.81	6.424	14.519	0.891	1.924	6.557
2	Small	60	2.755	6.458	14.887	0.807	1.986	10.627
2	Small	60	3.136	6.246	13.233	0.718	1.723	8.704
2	Small	90	1.892	5.996	17.019	0.687	1.578	4.017
2	Small	90	2.723	6.252	14.261	0.805	1.925	6.673
2	Small	90	2.84	6.372	14.471	0.661	1.696	5.404
2	Small	90	3.302	7.291	18.313	0.69	1.666	4.97
2	Small	90	2.698	6.27	14.288	0.718	1.811	8.448
5	Large	30	2.18	4.075	8.132	0.603	1.263	3.821
5	Large	30	1.979	4.277	9.412	0.576	1.266	4.083
5	Large	30	1.461	3.702	11.424	0.604	1.236	2.875
5	Large	30	1.867	4.19	9.614	0.69	1.466	4.138
5	Large	30	2.153	3.99	7.866	0.489	1.093	3.132
5	Large	60	1.979	3.615	7.318	0.345	0.777	2.04
5	Large	60	1.723	3.787	8.381	0.546	1.18	2.643
5	Large	60	1.218	3.168	11.031	0.345	0.718	1.523
5	Large	60	1.779	3.846	8.611	0.431	0.805	1.783
5	Large	60	1.788	3.741	7.999	0.517	1.091	2.787
5	Large	90	1.665	3.618	8.154	0.401	0.746	1.838
5	Large	90	1.09	2.611	11.36	0.344	0.746	1.779
5	Large	90	1.034	2.585	11.225	0.288	0.517	1.092
5	Large	90	1.605	3.614	8.324	0.257	0.688	1.722
5	Large	90	1.634	3.615	8.238	0.316	0.719	1.524
5	Medium	30	2.44	3.846	6.717	0.487	1.005	3.558
5	Medium	30	1.55	2.928	6.084	0.374	0.834	2.588
5	Medium	30	1.519	3.296	7.312	0.546	1.062	2.511
5	Medium	30	1.063	2.585	8.468	0.431	0.949	6.121
5	Medium	30	1.376	3.042	6.657	0.288	0.633	1.64
5	Medium	60	1.12	2.067	3.817	0.517	0.862	1.867
5	Medium	60	1.091	2.189	4.718	0.287	0.604	1.783
5	Medium	60	0.662	1.322	3.589	0.259	0.602	1.58
5	Medium	60	1.12	2.27	4.508	0.344	0.688	1.606
5	Medium	60	1.233	2.15	3.874	0.287	0.633	1.524
5	Medium	90	1.004	1.634	3.037	0.23	0.46	1.006
5	Medium	90	0.66	1.405	3.557	0.259	0.518	1.151
5	Medium	90	0.517	1.004	2.698	0.345	0.689	1.553
5	Medium	90	0.918	1.722	3.559	0.432	0.892	1.812

5	Medium	90	0.918	1.579	2.899	0.288	0.604	1.208
5	Small	30	1.466	2.614	4.797	0.403	0.891	2.213
5	Small	30	1.32	2.815	5.719	0.403	0.863	2.224
5	Small	30	0.918	1.864	5.716	0.374	0.747	1.753
5	Small	30	1.263	2.698	5.569	0.373	0.747	1.725
5	Small	30	1.776	2.902	4.998	0.345	0.69	1.495
5	Small	60	1.062	1.779	3.185	0.289	0.519	1.036
5	Small	60	0.92	1.867	3.762	0.374	0.719	1.953
5	Small	60	0.574	1.205	2.929	0.287	0.574	1.206
5	Small	60	0.891	1.866	3.819	0.259	0.661	1.868
5	Small	60	1.064	1.84	3.302	0.403	0.748	1.811
5	Small	90	0.861	1.436	2.583	0.26	0.547	1.065
5	Small	90	0.717	1.406	2.928	0.258	0.575	1.35
5	Small	90	0.372	0.717	1.911	0.316	0.632	1.586
5	Small	90	1.035	2.039	4.077	0.287	0.603	1.238
5	Small	90	1.204	2.123	3.787	0.201	0.373	0.946
6	Large	30	3.073	7.779	15.931	1.091	2.267	6.143
6	Large	30	3.817	8.897	17.422	0.689	1.636	5.368
6	Large	30	2.039	7.952	18.028	0.704	1.537	6.448
6	Large	30	4.276	10.098	20.294	0.718	1.609	5.855
6	Large	30	3.023	7.845	16.054	0.689	1.636	5.314
6	Large	60	2.869	7.002	14.263	0.746	1.35	3.504
6	Large	60	2.326	7.321	15.126	0.603	1.092	3.246
6	Large	60	1.674	6.699	15.173	0.603	1.234	4.421
6	Large	60	3.215	7.692	15.153	0.574	1.177	4.056
6	Large	60	2.669	7.062	14.534	0.546	1.12	3.649
6	Large	90	2.267	6.001	12.602	0.489	1.035	3.881
6	Large	90	3.385	7.058	13.575	0.648	1.223	3.693
6	Large	90	1.062	5.31	12.169	0.547	1.036	3.135
6	Large	90	1.926	6.029	12.701	0.402	0.891	3.082
6	Large	90	3.252	6.956	13.271	0.69	1.179	3.215
6	Medium	30	2.981	8.063	17.823	0.403	0.949	9.797
6	Medium	30	2.815	8.084	16.929	0.431	0.947	6.896
6	Medium	30	1.499	7.192	17.297	0.458	0.975	6.403
6	Medium	30	2.868	8.265	18.196	0.488	1.063	6.059
6	Medium	30	2.898	7.748	15.958	0.374	0.89	7.212
6	Medium	60	2.527	6.688	14.326	0.661	1.353	13.155
6	Medium	60	2.325	6.726	14.581	0.374	1.006	9.688
6	Medium	60	1.576	6.486	14.465	0.517	1.12	8.642
6	Medium	60	2.21	6.686	14.321	0.43	1.034	15.042
6	Medium	60	2.522	6.683	14.088	0.575	1.264	11.116

6	Medium	90	2.181	5.198	11.259	0.431	1.236	16.754
6	Medium	90	1.981	5.256	11.549	0.545	1.292	26.167
6	Medium	90	1.148	4.537	11.253	0.46	1.351	34.77
6	Medium	90	1.894	4.975	11.033	0.516	1.32	28.809
6	Medium	90	2.153	5.195	11.538	0.459	1.119	15.582
6	Small	30	2.554	6.919	15.271	0.574	1.233	5.254
6	Small	30	2.464	7.229	16.615	0.488	1.06	3.642
6	Small	30	1.433	6.716	15.222	0.487	1.09	8.102
6	Small	30	2.462	7.224	17.014	0.459	1.004	13.261
6	Small	30	2.584	6.841	14.915	0.516	1.118	14.58
6	Small	60	1.894	5.224	11.141	0.401	0.918	4.306
6	Small	60	1.782	5.225	11.223	0.461	0.977	9.968
6	Small	60	0.89	4.767	11.009	0.43	0.976	13.929
6	Small	60	0.89	4.927	12.245	0.487	1.004	6.145
6	Small	60	1.956	5.268	11.213	0.431	0.948	5.579
6	Small	90	1.578	4.22	9	0.488	0.976	5
6	Small	90	1.434	4.101	9.215	0.432	0.921	12.578
6	Small	90	0.782	3.597	9.742	0.417	0.935	20.041
6	Small	90	1.406	4.159	9.447	0.432	0.892	3.934
6	Small	90	1.58	4.279	9.56	0.402	0.861	13.662
8	Large	30	2.38	4.217	8.237	1.121	2.155	5.457
8	Large	30	2.268	4.42	8.84	1.12	2.155	5.426
8	Large	30	1.579	3.876	10.363	1.206	2.325	6.726
8	Large	30	2.328	4.478	8.842	1.107	2.172	5.744
8	Large	30	2.64	4.505	8.466	1.291	2.325	5.666
8	Large	60	2.134	3.597	6.617	0.718	1.38	3.335
8	Large	60	1.922	3.562	6.773	0.807	1.581	3.974
8	Large	60	1.149	2.672	7.033	0.719	1.437	3.739
8	Large	60	1.836	3.445	6.688	0.748	1.495	3.677
8	Large	60	2.065	3.528	6.515	0.833	1.639	4.112
8	Large	90	1.753	3.016	5.27	0.574	1.062	2.471
8	Large	90	0.918	2.01	4.394	0.574	1.264	3.474
8	Large	90	1.119	2.094	4.907	0.632	1.265	3.624
8	Large	90	1.435	2.726	5.223	0.575	1.235	3.475
8	Large	90	1.694	2.958	5.255	0.603	1.321	3.589
8	Medium	30	1.904	3.397	6.735	0.748	1.437	3.36
8	Medium	30	1.722	3.473	7.492	0.691	1.409	3.682
8	Medium	30	1.15	2.88	8.112	0.632	1.349	3.85
8	Medium	30	1.494	3.357	8.668	0.775	1.552	4.681
8	Medium	30	1.922	3.7	7.295	0.604	1.179	3.392
8	Medium	60	1.607	2.728	4.879	0.632	1.293	3.593

8	Medium	60	1.147	2.352	4.737	0.632	1.178	3.134
8	Medium	60	0.861	1.779	4.678	0.777	1.495	3.45
8	Medium	60	1.233	2.468	4.824	0.603	1.205	2.841
8	Medium	60	1.578	2.696	4.823	0.746	1.496	4.108
8	Medium	90	1.264	2.24	3.905	0.431	0.92	2.299
8	Medium	90	0.804	1.779	3.704	0.489	0.949	2.315
8	Medium	90	0.774	1.376	3.395	0.576	1.178	2.729
8	Medium	90	0.889	1.923	3.703	0.487	0.919	2.183
8	Medium	90	1.293	2.355	4.106	0.603	1.207	3.734
8	Small	30	2.212	3.879	7.468	0.718	1.436	3.687
8	Small	30	1.723	3.418	6.84	0.577	1.123	2.762
8	Small	30	1.587	3.625	9.423	0.603	1.292	3.275
8	Small	30	2.068	4.077	8.611	0.891	1.725	4.512
8	Small	30	2.152	3.761	7.119	0.576	1.15	2.708
8	Small	60	1.664	2.899	5.311	0.548	1.094	3.077
8	Small	60	1.147	2.381	4.994	0.489	1.006	2.528
8	Small	60	0.747	1.58	4.173	0.719	1.293	3.39
8	Small	60	1.176	2.418	5.003	0.431	0.92	2.155
8	Small	60	1.627	2.863	5.242	0.689	1.38	3.075
8	Small	90	0.89	1.779	3.502	0.345	0.833	1.868
8	Small	90	0.918	1.636	3.501	0.517	0.977	2.01
8	Small	90	0.574	1.12	2.755	0.488	1.179	2.874
8	Small	90	0.803	1.462	2.927	0.459	0.919	2.097
8	Small	90	0.889	1.721	3.156	0.546	0.978	1.992
9	Large	30	2.727	6.286	11.595	0.373	0.804	1.752
9	Large	30	1.752	4.712	9.565	0.343	0.688	1.407
9	Large	30	1.265	5.597	12.946	0.315	0.661	1.35
9	Large	30	2.41	6.514	12.544	0.23	0.489	1.12
9	Large	30	2.498	5.771	10.687	0.259	0.576	1.207
9	Large	60	1.724	1.724	7.518	0.2	0.401	0.774
9	Large	60	1.119	1.119	10.219	0.172	0.345	0.689
9	Large	60	1.147	1.147	10.772	0.2	0.373	0.718
9	Large	60	2.039	2.039	9.96	0.172	0.344	0.659
9	Large	60	1.693	1.693	6.862	0.202	0.403	0.776
9	Large	90	0.86	1.577	3.271	0.172	0.345	0.661
9	Large	90	1.894	4.937	9.299	0.172	0.317	0.633
9	Large	90	0.344	0.918	3.184	0.173	0.346	0.661
9	Large	90	0.373	0.746	2.067	0.182	0.384	0.757
9	Large	90	2.095	4.853	8.815	0.202	0.374	0.72
9	Medium	30	1.637	3.732	7.262	0.575	1.264	8.53
9	Medium	30	1.264	3.243	8.446	0.661	1.81	17.989

9	Medium	30	0.69	2.881	11.787	0.66	1.666	17.583
9	Medium	30	1.461	3.902	8.119	0.631	1.436	11.323
9	Medium	30	2.44	5.598	10.343	0.632	1.523	15.174
9	Medium	60	1.063	2.382	9.797	0.258	0.487	1.09
9	Medium	60	1.865	4.881	9.389	0.346	0.719	4.193
9	Medium	60	0.947	4.048	13.06	0.489	1.091	3.76
9	Medium	60	1.092	2.678	7.076	0.518	1.179	4.424
9	Medium	60	1.866	4.993	9.585	0.402	0.862	2.24
9	Medium	90	1.693	3.385	6.455	0.46	0.891	11.732
9	Medium	90	2.009	5.454	11.557	0.343	0.66	2.009
9	Medium	90	1.091	4.452	9.509	0.315	0.63	10.381
9	Medium	90	0.975	2.238	8.272	0.431	0.803	2.154
9	Medium	90	2.211	5.28	12.457	0.43	0.861	1.837
9	Small	30	1.032	1.922	4.249	0.374	0.805	1.955
9	Small	30	1.004	1.866	4.363	0.288	0.661	1.897
9	Small	30	0.43	1.291	5.978	0.374	0.803	14.675
9	Small	30	1.264	3.1	7.491	0.345	0.805	8.531
9	Small	30	1.551	3.187	11.805	0.372	0.832	25.202
9	Small	60	0.43	1.091	2.243	0.46	0.92	2.125
9	Small	60	0.66	1.176	2.869	0.431	0.862	1.724
9	Small	60	0.229	0.486	2.954	0.258	0.545	19.03
9	Small	60	0.43	1.205	2.639	0.517	1.178	4.883
9	Small	60	0.575	1.437	3.447	0.431	0.949	24.622
9	Small	90	0.344	0.918	2.037	0.201	0.43	1.179
9	Small	90	0.315	0.831	1.895	0.402	0.804	2.125
9	Small	90	0.286	0.629	2.151	0.602	1.274	14.921
9	Small	90	0.344	0.689	1.981	0.491	1.037	2.446
9	Small	90	0.862	1.522	3.158	0.546	1.122	2.989

Table A-2: Pressure data from breathing tests presented in Chapter 2. Standard deviations for tests presented include 9 breaths, repeated 3 times.

Subject	Flowrate (SLPM)	Cannula	Pmax (cmH2O)	Uncertainty	Pmin (cmH2O)	Uncertainty	Pmean (cmH2O)	Uncertainty	PEEP (cmH2O)	Uncertainty
2	0	Large	3.8365	0.029854	-3.5955	0.024146	0.049112	0.003882	-0.05097	0.017026
2	0	Medium	3.6287	0.031568	-3.4832	0.023081	0.024018	0.002332	-0.04318	0.026625
2	0	Small	3.646	0.031887	-3.5027	0.026306	0.019715	0.002331	-0.0501	0.024388
2	30	Large	5.9532	0.05808	-2.7514	0.025443	1.5092	0.007005	1.4544	0.057589
2	30	Medium	6.7031	0.14722	-2.6734	0.14938	1.9209	0.075579	1.8299	0.19235
2	30	Small	7.5597	0.055966	-2.3182	0.030853	2.7033	0.013805	2.9822	0.070784
2	60	Large	10.322	0.081826	0.3975	0.055287	5.322	0.051085	5.3359	0.13563
2	60	Medium	13.643	0.42309	1.3162	0.07827	7.1125	0.058789	6.7665	0.43077

2	60	Small	17.268	0.16074	3.9344	0.105	11.079	0.034544	11.786	0.067293
5	0	Large	1.583	0.020768	-1.4792	0.018209	0.017338	0.002032	-0.05498	0.027087
5	0	Medium	1.5379	0.020222	-1.4381	0.016293	0.018636	0.001386	-0.04883	0.022427
5	0	Small	1.5167	0.022112	-1.4313	0.025015	0.015937	0.001993	-0.05132	0.032113
5	30	Large	3.3787	0.033719	-0.85028	0.024905	1.2463	0.010834	1.266	0.043205
5	30	Medium	4.4318	0.12634	-0.87185	0.025588	1.5581	0.009569	1.3781	0.20946
5	30	Small	5.0525	0.042011	-0.90359	0.031003	2.0943	0.011696	2.3631	0.10469
5	60	Large	7.3841	0.060122	1.7655	0.042318	4.6151	0.009538	4.6917	0.11761
5	60	Medium	11.414	0.61769	1.76	0.04951	5.9104	0.066827	5.9333	0.91135
5	60	Small	14.525	0.071395	2.1667	0.14101	8.499	0.031158	9.3144	0.23266
6	0	Large	7.816	0.039353	-7.0906	0.026146	0.1213	0.003951	-0.05325	0.016811
6	0	Medium	7.7595	0.033721	-7.0691	0.030118	0.10979	0.0031	-0.06104	0.018317
6	0	Small	7.7662	0.032471	-7.0656	0.058202	0.11414	0.002982	-0.05305	0.02
6	30	Large	8.7857	0.04481	-6.6074	0.040443	0.84825	0.005715	0.69332	0.023984
6	30	Medium	9.1149	0.31852	-6.4591	0.042062	1.0143	0.023757	0.75379	0.095903
6	30	Small	10.135	0.033904	-6.2069	0.0401	1.8235	0.010618	1.8652	0.075382
6	60	Large	11.266	0.048911	-5.1087	0.043871	2.8888	0.0045	2.7983	0.088241
6	60	Medium	15.374	0.53899	-4.0344	0.47811	5.0397	0.19567	4.6491	1.3497
6	60	Small	15.815	0.47094	-2.607	0.12654	6.6892	0.27798	7.0498	0.46285
8	0	Large	1.6813	0.015279	-1.5615	0.012899	0.018501	0.001563	-0.05001	0.015689
8	0	Medium	1.5658	0.021915	-1.4967	0.022769	0.008769	0.002156	-0.04618	0.018817
8	0	Small	1.5916	0.017841	-1.516	0.019247	0.010875	0.001614	-0.04281	0.022107
8	30	Large	2.879	0.036973	-1.0261	0.020538	0.93291	0.007661	0.99225	0.061361
8	30	Medium	5.5673	0.098942	-0.18804	0.047416	2.61	0.014432	2.5757	0.18471
8	30	Small	4.1475	0.074683	-0.26468	0.04672	1.9294	0.008048	1.9467	0.076353
8	60	Large	5.8478	0.068105	0.63635	0.035798	3.3445	0.008488	3.5285	0.11214
8	60	Medium	14.856	0.24776	3.3698	0.1981	9.0658	0.044852	9.911	0.2793
8	60	Small	11.379	0.12104	4.0069	0.072393	7.639	0.016547	7.6252	0.25264
9	0	Large	3.7507	0.061259	-3.6082	0.031783	0.028189	0.005963	-0.05348	0.012767
9	0	Medium	3.6513	0.06428	-3.5544	0.054897	0.020591	0.006749	-0.05196	0.016119
9	0	Small	3.6707	0.067836	-3.5678	0.033523	0.019949	0.006705	-0.05086	0.025246
9	30	Large	4.786	0.07645	-3.074	0.032441	0.78148	0.004336	0.67821	0.035708
9	30	Medium	5.1856	0.058488	-2.9267	0.030441	1.0569	0.008942	0.96584	0.03152
9	30	Small	5.8863	0.076835	-2.4806	0.044769	1.6845	0.009736	1.6872	0.035326
9	60	Large	7.1737	0.068094	-1.5101	0.042733	2.7881	0.009116	2.7379	0.02082
9	60	Medium	8.7206	0.13402	-0.82261	0.14832	3.924	0.053575	3.9384	0.11013
9	60	Small	11.589	0.11428	1.1541	0.066184	6.3761	0.013279	6.41	0.12205

## Appendix B Raw Data for Chapter 3

Table B-1: Clearance and Pressure data from breathing tests presented in Chapter 3. Standard deviations for tests presented include 9 breaths, repeated 3 times.

Subject	Gas	Cannula	Flow (SLPM)	Average CO2 (%)	SD (%)	PEEP (cmH2O)	SD (cmH2O)
2	Air	Generic	0	1.9009	0.055984	-0.01837	0.007632
2	Air	Generic	15	1.7478	0.027238	0.41054	0.016626
2	Air	Generic	30	1.6822	0.031024	1.6812	0.11997
2	Air	Generic	60	1.6013	0.032485	6.616	0.29156
2	Air	Vapotherm Adult	0	1.9034	0.04255	-0.01642	0.008468
2	Air	Vapotherm Adult	15	1.7367	0.036953	0.80594	0.012687
2	Air	Vapotherm Adult	30	1.6382	0.031467	3.1242	0.042382
2	Air	Vapotherm Adult	60	1.533	0.043756	11.506	0.11674
2	Air	Vapotherm Adult S	0	1.8748	0.033003	-0.02395	0.010238
2	Air	Vapotherm Adult Small	15	1.7012	0.042088	0.85096	0.023096
2	Air	Vapotherm Adult Small	30	1.6183	0.029209	3.4562	0.065151
2	Air	Vapotherm Adult Small	60	1.5084	0.035585	13.989	0.20239
2	He/O2	Generic	0	1.9009	0.055984	-0.01837	0.007632
2	He/O2	Generic	15	1.7323	0.04962	0.10327	0.00984
2	He/O2	Generic	30	1.6836	0.045358	0.39578	0.011154
2	He/O2	Generic	60	1.6015	0.041382	1.6005	0.060185
2	He/O2	Vapotherm Adult	0	1.9034	0.04255	-0.01642	0.008468
2	He/O2	Vapotherm Adult	15	1.7263	0.037771	0.18438	0.008955
2	He/O2	Vapotherm Adult	30	1.6811	0.046469	0.68079	0.007036
2	He/O2	Vapotherm Adult	60	1.5778	0.034216	2.5568	0.019932
2	He/O2	Vapotherm Adult S	0	1.8748	0.033003	-0.02395	0.010238
2	He/O2	Vapotherm Adult Small	15	1.7651	0.054979	0.21563	0.009283
2	He/O2	Vapotherm Adult Small	30	1.6925	0.042569	0.84838	0.016427
2	He/O2	Vapotherm Adult Small	60	1.6068	0.037458	3.4829	0.020037
2	Oxygen	Generic	0	1.9009	0.055984	-0.01837	0.007632
2	Oxygen	Generic	15	1.6944	0.066207	0.44748	0.029645
2	Oxygen	Generic	30	1.538	0.027481	1.7241	0.077511
2	Oxygen	Generic	60	1.4447	0.034373	7.023	0.36066
2	Oxygen	Vapotherm Adult	0	1.9034	0.04255	-0.01642	0.008468
2	Oxygen	Vapotherm Adult	15	1.6716	0.057667	0.77961	0.013531
2	Oxygen	Vapotherm Adult	30	1.5407	0.040881	3.009	0.037036
2	Oxygen	Vapotherm Adult	60	1.4396	0.039934	11.526	0.07097
2	Oxygen	Vapotherm Adult S	0	1.8748	0.033003	-0.02395	0.010238
2	Oxygen	Vapotherm Adult Small	15	1.6612	0.034107	1.0425	0.021489

2	Oxygen	Vapotherm Adult Small	30	1.5306	0.034294	4.2349	0.062978
2	Oxygen	Vapotherm Adult Small	60	1.4654	0.060804	16.78	0.13125
5	Air	Generic	0	2.0166	0.035805	-0.02642	0.006804
5	Air	Generic	15	1.7862	0.031856	0.38458	0.025543
5	Air	Generic	30	1.7242	0.028732	1.7909	0.13006
5	Air	Generic	60	1.6206	0.034979	7.0119	0.29266
5	Air	Vapotherm Adult	0	2.0467	0.038851	-0.03098	0.007628
5	Air	Vapotherm Adult	15	1.8171	0.029095	0.65918	0.010392
5	Air	Vapotherm Adult	30	1.6998	0.027398	2.5815	0.036793
5	Air	Vapotherm Adult	60	1.5805	0.047187	9.8878	0.15584
5	Air	Vapotherm Adult S	0	2.0599	0.039101	-0.02447	0.007702
5	Air	Vapotherm Adult Small	15	1.8342	0.041008	0.72744	0.028075
5	Air	Vapotherm Adult Small	30	1.7078	0.031802	2.7307	0.058889
5	Air	Vapotherm Adult Small	60	1.6066	0.046606	9.8807	0.19343
5	He/O2	Generic	0	2.0166	0.035805	-0.02642	0.006804
5	He/O2	Generic	15	1.6065	0.032249	0.095722	0.010097
5	He/O2	Generic	30	1.4792	0.029949	0.38506	0.019538
5	He/O2	Generic	60	1.3476	0.023629	1.2402	0.026078
5	He/O2	Vapotherm Adult	0	2.0467	0.038851	-0.03098	0.007628
5	He/O2	Vapotherm Adult	15	1.8376	0.045842	0.15748	0.007283
5	He/O2	Vapotherm Adult	30	1.6949	0.031792	0.60902	0.010365
5	He/O2	Vapotherm Adult	60	1.5879	0.031969	2.3293	0.017829
5	He/O2	Vapotherm Adult S	0	2.0599	0.039101	-0.02447	0.007702
5	He/O2	Vapotherm Adult Small	15	1.6588	0.02955	0.17247	0.008641
5	He/O2	Vapotherm Adult Small	30	1.5507	0.040008	0.68618	0.017639
5	He/O2	Vapotherm Adult Small	60	1.4188	0.027268	2.6175	0.037303
5	Oxygen	Generic	0	2.0166	0.035805	-0.02642	0.006804
5	Oxygen	Generic	15	1.7572	0.03257	0.40141	0.022065
5	Oxygen	Generic	30	1.6514	0.031377	1.86	0.06147
5	Oxygen	Generic	60	1.5395	0.032274	7.3949	0.38052
5	Oxygen	Vapotherm Adult	0	2.0467	0.038851	-0.03098	0.007628
5	Oxygen	Vapotherm Adult	15	1.7297	0.032979	0.76189	0.012987
5	Oxygen	Vapotherm Adult	30	1.5932	0.025803	2.9593	0.033438
5	Oxygen	Vapotherm Adult	60	1.5075	0.054456	11.307	0.11094
5	Oxygen	Vapotherm Adult S	0	2.0599	0.039101	-0.02447	0.007702
5	Oxygen	Vapotherm Adult Small	15	1.7617	0.025862	0.86722	0.016868
5	Oxygen	Vapotherm Adult Small	30	1.6149	0.020756	3.3479	0.049985
5	Oxygen	Vapotherm Adult Small	60	1.4926	0.038263	12.545	0.17829
6	Air	Generic	0	1.7765	0.065892	-0.01233	0.007457
6	Air	Generic	15	1.6143	0.039213	0.35703	0.013866
6	Air	Generic	30	1.5466	0.032032	1.3479	0.063067

6	Air	Generic	60	1.4779	0.024624	3.5552	0.19431
6	Air	Vapotherm Adult	0	1.875	0.047516	-0.017	0.00679
6	Air	Vapotherm Adult	15	1.6339	0.038395	0.49566	0.011344
6	Air	Vapotherm Adult	30	1.5726	0.039371	1.914	0.029367
6	Air	Vapotherm Adult	60	1.4936	0.03653	6.2517	0.080716
6	Air	Vapotherm Adult S	0	1.8645	0.039225	-0.01509	0.007195
6	Air	Vapotherm Adult Small	15	1.6164	0.03021	0.38786	0.016727
6	Air	Vapotherm Adult Small	30	1.5466	0.037405	1.4858	0.030168
6	Air	Vapotherm Adult Small	60	1.4941	0.034136	5.9021	0.1133
6	He/O2	Generic	0	1.7765	0.065892	-0.01233	0.007457
6	He/O2	Generic	15	1.6015	0.044069	0.038933	0.006102
6	He/O2	Generic	30	1.5293	0.043654	0.30968	0.013133
6	He/O2	Generic	60	1.4027	0.030764	0.92963	0.018267
6	He/O2	Vapotherm Adult	0	1.875	0.047516	-0.017	0.00679
6	He/O2	Vapotherm Adult	15	1.6272	0.046224	0.13027	0.006859
6	He/O2	Vapotherm Adult	30	1.5387	0.037152	0.51521	0.010391
6	He/O2	Vapotherm Adult	60	1.4128	0.037066	1.9136	0.016172
6	He/O2	Vapotherm Adult S	0	1.8645	0.039225	-0.01509	0.007195
6	He/O2	Vapotherm Adult Small	15	1.5935	0.042124	0.11557	0.008666
6	He/O2	Vapotherm Adult Small	30	1.4657	0.039008	0.42538	0.010774
6	He/O2	Vapotherm Adult Small	60	1.3753	0.027779	1.5435	0.026716
6	Oxygen	Generic	0	1.7765	0.065892	-0.01233	0.007457
6	Oxygen	Generic	15	1.5757	0.043901	0.37755	0.019831
6	Oxygen	Generic	30	1.5051	0.023921	1.3892	0.055117
6	Oxygen	Generic	60	1.4129	0.029363	5.3292	0.14584
6	Oxygen	Vapotherm Adult	0	1.875	0.047516	-0.017	0.00679
6	Oxygen	Vapotherm Adult	15	1.5602	0.035995	0.52554	0.021718
6	Oxygen	Vapotherm Adult	30	1.4749	0.034751	2.0435	0.023923
6	Oxygen	Vapotherm Adult	60	1.3839	0.042916	7.0995	0.21755
6	Oxygen	Vapotherm Adult S	0	1.8645	0.039225	-0.01509	0.007195
6	Oxygen	Vapotherm Adult Small	15	1.5634	0.04534	0.46299	0.017705
6	Oxygen	Vapotherm Adult Small	30	1.4529	0.035721	1.4891	0.031048
6	Oxygen	Vapotherm Adult Small	60	1.3915	0.036839	5.8481	0.077772
8	Air	Generic	0	1.979	0.047246	-0.01845	0.009452
8	Air	Generic	15	1.7821	0.048676	0.7737	0.03717
8	Air	Generic	30	1.6596	0.030711	2.9311	0.23741
8	Air	Generic	60	1.5751	0.027819	9.2126	0.53649
8	Air	Vapotherm Adult	0	2.0255	0.050787	-0.02029	0.011119
8	Air	Vapotherm Adult	15	1.8636	0.033077	0.6643	0.019725
8	Air	Vapotherm Adult	30	1.7744	0.043441	2.5232	0.039508
8	Air	Vapotherm Adult	60	1.6899	0.076053	9.2662	0.10844

8	Air	Vapotherm Adult S	0	2.0397	0.049017	-0.02388	0.008809
8	Air	Vapotherm Adult Small	15	1.8745	0.03312	0.7704	0.029507
8	Air	Vapotherm Adult Small	30	1.7493	0.02872	2.6954	0.078903
8	Air	Vapotherm Adult Small	60	1.6464	0.047911	10.086	0.15763
8	He/O2	Generic	0	1.979	0.047246	-0.01845	0.009452
8	He/O2	Generic	15	1.9334	0.087129	0.18647	0.007145
8	He/O2	Generic	30	1.8014	0.10085	0.7609	0.03067
8	He/O2	Generic	60	1.6582	0.088212	1.3857	0.13898
8	He/O2	Vapotherm Adult	0	2.0255	0.050787	-0.02029	0.011119
8	He/O2	Vapotherm Adult	15	1.8623	0.048259	0.13639	0.007246
8	He/O2	Vapotherm Adult	30	1.795	0.044834	0.54231	0.009132
8	He/O2	Vapotherm Adult	60	1.6074	0.032861	2.0907	0.027821
8	He/O2	Vapotherm Adult S	0	2.0397	0.049017	-0.02388	0.008809
8	He/O2	Vapotherm Adult Small	15	1.8689	0.057895	0.1417	0.006319
8	He/O2	Vapotherm Adult Small	30	1.8145	0.097878	0.70307	0.010951
8	He/O2	Vapotherm Adult Small	60	1.5847	0.044127	2.9455	0.018818
8	Oxygen	Generic	0	1.979	0.047246	-0.01845	0.009452
8	Oxygen	Generic	15	1.7728	0.049581	0.68531	0.086016
8	Oxygen	Generic	30	1.6063	0.030492	3.154	0.21882
8	Oxygen	Generic	60	1.5129	0.039288	9.1513	0.46205
8	Oxygen	Vapotherm Adult	0	2.0255	0.050787	-0.02029	0.011119
8	Oxygen	Vapotherm Adult	15	1.8051	0.045275	0.73886	0.015088
8	Oxygen	Vapotherm Adult	30	1.6787	0.04099	2.7469	0.055048
8	Oxygen	Vapotherm Adult	60	1.6041	0.070224	10.245	0.11515
8	Oxygen	Vapotherm Adult S	0	2.0397	0.049017	-0.02388	0.008809
8	Oxygen	Vapotherm Adult Small	15	1.8096	0.032677	0.95274	0.020459
8	Oxygen	Vapotherm Adult Small	30	1.6591	0.04649	3.9107	0.053426
8	Oxygen	Vapotherm Adult Small	60	1.5256	0.043864	14.857	0.14007
9	Air	Generic	0	1.9155	0.066434	-0.01748	0.007512
9	Air	Generic	15	1.6957	0.035461	0.20857	0.00958
9	Air	Generic	30	1.6258	0.026249	0.89297	0.026476
9	Air	Generic	60	1.5926	0.037529	3.38	0.11922
9	Air	Vapotherm Adult	0	1.9343	0.054987	-0.01824	0.007582
9	Air	Vapotherm Adult	15	1.6802	0.030458	0.28579	0.005467
9	Air	Vapotherm Adult	30	1.6093	0.03927	1.1038	0.017294
9	Air	Vapotherm Adult	60	1.5796	0.033861	4.1754	0.057587
9	Air	Vapotherm Adult S	0	1.9104	0.037553	-0.0223	0.007281
9	Air	Vapotherm Adult Small	15	1.6651	0.03781	0.35417	0.013162
9	Air	Vapotherm Adult Small	30	1.6034	0.028826	1.2017	0.023811
9	Air	Vapotherm Adult Small	60	1.5594	0.028716	4.342	0.055
9	He/O2	Generic	0	1.9155	0.066434	-0.01748	0.007512

9	He/O2	Generic	15	1.6058	0.045309	0.040527	0.006468
9	He/O2	Generic	30	1.5067	0.039749	0.19631	0.011101
9	He/O2	Generic	60	1.4511	0.035789	0.76152	0.018599
9	He/O2	Vapotherm Adult	0	1.9343	0.054987	-0.01824	0.007582
9	He/O2	Vapotherm Adult	15	1.6204	0.044955	0.045848	0.00807
9	He/O2	Vapotherm Adult	30	1.5189	0.042753	0.19768	0.008283
9	He/O2	Vapotherm Adult	60	1.4676	0.035994	0.77944	0.009433
9	He/O2	Vapotherm Adult S	0	1.9104	0.037553	-0.0223	0.007281
9	He/O2	Vapotherm Adult Small	15	1.6288	0.049302	0.076664	0.010398
9	He/O2	Vapotherm Adult Small	30	1.5149	0.047019	0.29005	0.0101
9	He/O2	Vapotherm Adult Small	60	1.4594	0.048067	1.1183	0.012775
9	Oxygen	Generic	0	1.9155	0.066434	-0.01748	0.007512
9	Oxygen	Generic	15	1.6081	0.031789	0.28737	0.013361
9	Oxygen	Generic	30	1.4977	0.026394	1.1608	0.026271
9	Oxygen	Generic	60	1.4434	0.029073	4.1088	0.20767
9	Oxygen	Vapotherm Adult	0	1.9343	0.054987	-0.01824	0.007582
9	Oxygen	Vapotherm Adult	15	1.5785	0.028776	0.31644	0.016669
9	Oxygen	Vapotherm Adult	30	1.4916	0.037938	1.2082	0.016137
9	Oxygen	Vapotherm Adult	60	1.4548	0.033309	4.536	0.053964
9	Oxygen	Vapotherm Adult S	0	1.9104	0.037553	-0.0223	0.007281
9	Oxygen	Vapotherm Adult Small	15	1.6136	0.04017	0.48749	0.040972
9	Oxygen	Vapotherm Adult Small	30	1.5008	0.02652	1.5493	0.023013
9	Oxygen	Vapotherm Adult Small	60	1.4464	0.03385	3.4221	0.044858